

20000731153

AD _____

TEST PLANNING, COLLECTION AND ANALYSIS
OF PRESSURE DATA RESULTING FROM ARMY
WEAPON SYSTEMS. VOL II - MODELING OF
FAR FIELD DATA

AD A118290

Final Report

J. Stuhmiller
F. Chan
P. Masiello
K. Tani

Reproduced From
Best Available Copy

April 1980

Supported by
US Army Medical Research and Development Command
Fort Detrick
Frederick, MD 21701

Contract No. DAMD17-78-C-8087

JAYCOR
1401 Camino Del Mar
Del Mar, CA 92014

Copy available to DTIC does not
permit fully legible reproduction

DTIC
ELECTE
AUG 17 1982
S D F

DOD Distribution Statement: Approved for Public Release; Distribution Unlim-
ited

The findings in this report are not to be construed as an official Department
of the Army position unless so designated by other authorized documents.

82 08 17 007

DTIC FILE COPY

DISCLAIMER NOTICE

**THIS DOCUMENT IS BEST QUALITY
PRACTICABLE. THE COPY FURNISHED
TO DTIC CONTAINED A SIGNIFICANT
NUMBER OF PAGES WHICH DO NOT
REPRODUCE LEGIBLY.**

REPORT DOCUMENTATION PAGE		READ INSTRUCTIONS BEFORE COMPLETING FORM
1. REPORT NUMBER	2. GOVT ACCESSION NO. A118290	3. RECIPIENT'S CATALOG NUMBER
4. TITLE (and Subtitle) TEST PLANNING, COLLECTION AND ANALYSIS OF PRESSURE DATA RESULTING FROM ARMY WEAPON SYSTEMS - VOL II - MODELING OF FAR FIELD DATA		5. TYPE OF REPORT & PERIOD COVERED Final Report September 1979-April 1980
7. AUTHOR(s) Dr. J. Stuhmiller Ms. K. Tani Dr. F. Chan Dr. P. Masiello		6. PERFORMING ORG. REPORT NUMBER
9. PERFORMING ORGANIZATION NAME AND ADDRESS JAYCOR 1401 Camino Del Mar Del Mar, CA 92014		8. CONTRACT OR GRANT NUMBER(s) DAMD 17-78-C-8087
11. CONTROLLING OFFICE NAME AND ADDRESS US Army Medical Research and Development Command Fort Detrick Frederick, MD 21701		10. PROGRAM ELEMENT, PROJECT, TASK AREA & WORK UNIT NUMBERS 61102A.3M161102BSG1.00.064
14. MONITORING AGENCY NAME & ADDRESS (if different from Controlling Office)		12. REPORT DATE April 1980
		13. NUMBER OF PAGES 69
		15. SECURITY CLASS. (of this report) Unclassified
		15a. DECLASSIFICATION/DOWNGRADING SCHEDULE
16. DISTRIBUTION STATEMENT (of this Report) Approved for Public Release; Distribution Unlimited.		
17. DISTRIBUTION STATEMENT (of the abstract entered in Block 20, if different from Report)		
18. SUPPLEMENTARY NOTES		
19. KEY WORDS (Continue on reverse side if necessary and identify by block number) Gun Blast Far Field Analysis Mathematical Formulation Mathematical Model of the Lung M-198 Howitzer with M-203 Charge Gun Blast and Ground Reflections		
20. ABSTRACT (Continue on reverse side if necessary and identify by block number) JAYCOR determined that much of the pressure trace detail from the M-198 155mm howitzer with the M203 charge could be understood in terms of gas dynamics and the gun and ground geometry. The objective was to determine the feasibility of stimulating the far field muzzle blast and to interpret the field data already taken. A lung model was also developed which gives a way of comparing various pressure traces in terms of the internal dynamics. The agreement seen between measured and predicted pressure traces is repeated in the lung response.		

Jan 83

SUMMARY

This report provides a prediction of the far field overpressure encountered near the M-198 155mm howitzer when fired with charge M203. The purpose of this effort was to determine the feasibility of simulating the far field muzzle blast in terms of gas dynamics and to correlate the pressures with field trial data. The results are extremely encouraging. The use of gas dynamics to understand the physical phenomena and subsequent predictions of pressure and energy fields in the far field is a natural extension applicable to many weapon systems.

DTIC
COPY
INSPECTED
2

Accession For	
NTIS GRA&I	<input checked="" type="checkbox"/>
DTIC TAB	<input type="checkbox"/>
Unannounced	<input type="checkbox"/>
Justification	
By _____	
Distribution/	
Availability Codes	
Dist	Avail and/or Special
A 23	CP

CONTENTS

	<u>Page</u>
1. INTRODUCTION	1
1.1 Background	1
1.2 Objective of JAYCOR's Analytical Effort	1
1.3 Technical Approach	1
1.4 Major Results	2
1.5 Recommendations	3
2. DISCUSSION OF RESULTS	5
APPENDICES	
A. GUN BLAST FAR FIELD ANALYSIS	A-1
A.1 Introduction	A-1
A.2 Mathematical Formulation	A-4
B. MATHEMATICAL MODE OF LUNG	B-1
B.1 Introduction	B-1
B.2 Mathematical Formulation	B-1
REFERENCES	R-1
CONTRACT PUBLICATIONS AND PERSONNEL	P-1
DISTRIBUTION	D-1

ILLUSTRATIONS

	<u>Page</u>
1. Ground map for locations of measurement	6
2. Measured and calculated pressure traces along B-line at 45° gun elevation	7
3. Variation of p_1 , p_2/p_1 and Δt with distance along B-line with 45° gun elevation	9
4. Lung pressure traces based on measured and calculated blast pressures along B-line at 45° gun elevation	10
5. Change of gaseous volume of lung based on measured and calculated blast pressures along B-line at 45° gun elevation	11
6. Measured and calculated pressure traces along C-line at 45° gun elevation	13
7. Variation of p_1 , p_2/p_1 and Δt with distance along C-line with 45° gun elevation	14
8. Lung pressure traces based on measured and calculated blast pressures along C-line at 45° gun elevation	15
9. Change of gaseous volume of lung based on measured and calculated blast pressures along C-line at 45° gun elevation	16
10. Measured pressure traces and their resulting lung pressures and changes of lung volume at C22 with 45° gun elevation	17
11. Measured and calculated pressure traces and their resulting lung pressures and changes of lung volume at D60 with 45° gun elevation	18
12. Measured and calculated pressure traces along B-line at 15° gun elevation	19
13. Variation of p_1 , p_2/p_1 and Δt with distance along B-line with 15° gun elevation	20
14. Lung pressure traces based on measured and calculated blast pressures along B-line at 15° gun elevation	21
15. Change of gaseous volume of lung based on measured and calculated blast pressures along B-line at 15° gun elevation	22
16. Measured and calculated pressure traces along C-line at 15° gun elevation	23

	<u>Page</u>
17. Variation of p_1 , p_2/p_1 and Δt with distance along C-line with 15° gun elevation	24
18. Lung pressure traces based on measured and calculated blast pressures along C-line at 15° gun elevation	25
19. Change of gaseous volume of lung based on measured and calculated blast pressures along C-line at 15° gun elevation	26
20. Measured pressure traces and their resulting lung pressures and changes of lung volume at C22 with 15° gun elevation	27
21. Measured and calculated pressure traces and their resulting lung pressures and changes of lung volume at D60 with 15° gun elevation	28
22. Measured and calculated pressure traces at C22 with 15° gun elevation	30
23. Variation of p_1 , p_2/p_1 and Δt with height at C22 with 15° gun elevation	31
24. Measured and calculated pressure traces along 0°-line at 45° gun elevation	32
25. Variation of p_1 , p_2/p_1 and Δt with distance along 0°-line with 45° gun elevation	33
26. Measured and calculated pressure traces along 30°-line at 45° gun elevation	34
27. Variation of p_1 , p_2/p_1 and Δt with distance along 30°-line with 45° gun elevation	35
28. Measured and calculated pressure traces along 60°-line at 45° gun elevation	36
29. Variation of p_1 , p_2/p_1 and Δt with distance along 60°-line with 45° gun elevation	37
30. Measured and calculated pressure traces along 90°-line at 45° gun elevation	38
31. Variation of p_1 , p_2/p_1 and Δt with distance along 90°-line with 45° gun elevation	39
32. Measured and calculated pressure traces along 120°-line at 45° gun elevation	40

	<u>Page</u>
33. Variation of p_1 , p_2/p_1 and Δt with distance along 120° -line with 45° gun elevation	41
34. Measured and calculated pressure traces along 150° -line at 45° gun elevation	42
35. Variation of p_1 , p_2/p_1 and Δt with distance along 150° -line with 45° gun elevation	43
36. Comparison of calculated and measured p_1 in the field at 45° gun elevation	44
37. Spatial pressure distribution in blast wave	A-1
38. Pressure trace variation with source strength	A-2
39. Spherical coordinates with origin at center of muzzle brake	A-5
40. Characteristics in r-t plane	A-9
41. Flow chart for the method of characteristics	A-10
42. Paths of incident and reflected waves	A-11
43. Definition sketch of lung model	B-2

1. INTRODUCTION

1.1 BACKGROUND

As part of the gun blast overpressure program, WRAIR had collected and analyzed statistically a considerable number of time pressure traces of the blast field in the neighborhood of the M198. Despite the considerable effort that had been expended, there were still several questions that hindered the further progress of quantifying crew exposure. Were the several peaks seen in the data due to ground reflections, multiple bursts, reflections of the gun body, or characteristics of the instrumentation? How could shot-to-shot repeatability be quantified? How could the Lovelace shock tube experiments be compared with the actual gun firings? Should dynamic as well as static pressures be compared? The answer to these questions seemed to lie in a better understanding of the physical phenomena of the blast field.

1.2 OBJECTIVE OF JAYCOR'S ANALYTICAL EFFORT

Because JAYCOR was already actively involved in the gun blast overpressure program, both in assisting in data collection and analysis, and because JAYCOR has a strong group in fluid dynamics, WRAIR decided to pursue a limited analysis of the phenomena. Based on those considerations, JAYCOR determined that much of the pressure trace detail could be understood in terms of gas dynamics and the gun and ground geometry. The objective of this initial phase was to determine the feasibility of simulating the far field muzzle blast and to interpret the field data already taken.

1.3 TECHNICAL APPROACH

It was decided to treat the blast as an independent spherical disturbance for each propagation direction away from the muzzle. Each disturbance would be characterized by a different energy deposition, the angular nonuniformity being due to the action of the muzzle brake geometry. For the purposes of demonstrating feasibility, the angular distribution was chosen by comparing with experimental data. Later, the distribution could be found directly from the charge characteristics, ballistics, and muzzle brake geometry.

The method of characteristics was chosen to integrate the time-dependent, gas dynamics equations because of its ability to accurately represent the sharp wave front. Ground reflections were taken to be given by perfect superposition, but work has also begun on an exact treatment of the non-linear effects.

The initial effort was focussed on the physical character of the blast, but when the results were shown to be so encouraging the pressure prediction model was coupled to a model of the lung and chest cavity.

In addition, the various models, including simple ones for the burn chemistry and shell dynamics, were combined into an overall system description with input quantities that are actually controllable, such as gun elevation, charge strength, muzzle geometry, and output quantities of interest to the overpressure program, such as pressure time histories and lung dynamics. Many of the models are in the earliest stages of development but putting them all together allows the sensitivity of each to be determined and gives a basic tool into which future improvements can be added.

1.4 MAJOR RESULTS

The principal features of the pressure traces can be understood in terms of intermediate strength gas dynamics disturbances, ground reflections, and the geometric relationship between the gun and the measuring station. The jaggedness of the measured signal is not contained in the present model and the duration of the pressure undershoot is not as great as that measured. For the cases tested, the simulation indicates the correct trend of pressure peaks and timings when distance, angle, height above ground, and gun elevation are varied. The qualitative shapes of the pressure signals are reproduced throughout the measurement field.

The lung model gives a way of comparing various pressure traces in terms of the internal dynamics. The agreement seen between measured and predicted pressure traces is repeated in the lung response. Thus, the differences in pressure traces does not significantly change the lung dynamics adding confidence to the simulation method.

In short, several independent tests indicate that the major physical phenomena are captured in this approximate approach.

1.5 RECOMMENDATIONS

The present phase of the work was only intended to demonstrate the feasibility of simulation in assisting the gun blast overpressure program and to obtain preliminary verification. It would be natural to extend the work by subjecting the models to detailed verification and then useful application. The items below are some of the areas that could profitably be pursued. The first group concerns the simulation of the blast field.

(1) The present effort has compared simulation with field test data for only about 20% of the shots measured. Procedures have been developed for efficiently handling all of the data, so that the validation can be made complete.

(2) Although the ideal ground reflection approximation appears to be adequate, the analysis of the nonlinear effects already begun should be finished because the crew stands in an area where this is most likely to be important.

(3) In the present treatment the angular distribution of energy caused by the muzzle brake is determined empirically from the field data itself. BRL is working on detailed calculations of the flow within the brake that can eventually supply a more fundamentally determined distribution. There will always be a need for a simple, but quantitative relation based on the brake geometry, however, and JAYCOR has several approaches that could yield engineering quality results in a relatively short time.

(4) Investigation into the origin of the apparently random pressure spikes should be made to complete the understanding of the physical phenomena. Effects that could be simulated and compared with data include randomness in the source and response of the instrument stands. This noise component does not seem to affect the qualitative features of the signal other than its jaggedness, but the apparently random superposition can occasionally increase the pressure peaks considerably and it would be useful to quantify the probability of occurrence.

(5) The application of the system code, that is the collection of engineering models from the explosion in the powder chamber, shell ballistics, brake redistribution, far field propagation, and lung response, should be pursued further. It is possible that the remaining discrepancies between the prediction and data, mainly the shape of the rarefaction, will be removed by solving the correct time-dependent, boundary-value problem for the far field rather than the present initial value problem.

(6) The system description could be applied to other weapon systems with suspected overpressure problems to further validate the concepts in those cases where data exists and to estimate the overpressure field where testing has not been done.

The second group concerns making use of the validated simulation to directly answer biomedical questions.

(7) An accurate and complete description of the blast field in the vicinity of the M198 and M109 to animal placement, future test instrumentation, and test environment.

(8) A quantitative determination if blasts from shock tubes are equivalent to those of the gun from the point of view of lung response.

(9) An estimate of internal organ dynamics (such as chest wall acceleration) to guide placement and specification of instrumentation in animal tests.

(10) An interpretation of the dynamics measured under test conditions in terms of a fluid-mechanical model of the organ so that the results can be extrapolated to other situations and to man.

2. DISCUSSION OF RESULTS

In order to demonstrate the feasibility of numerical simulation, we compare our calculated results with those of the measured gun blast overpressure data for M198 Howitzer and M-203 charge, collected on November 30, 1978 and May 15, 1979 at Aberdeen Proving Grounds. The comparison is arranged in a systematical way so that the various effects, such as the variation of the distance away from the muzzle brake, the angular variation of the measured positions, the variation of the height of the measured positions, and the variation of the gun elevation on the pressure traces can be analyzed. Subsequently, we compare the results obtained from the simulation of lung response on the crew positions, based on the calculated pressure traces and the measured ones, respectively. The method to calculate the pressure waves and the lung simulation will be described in the appendix.

A ground map showing the measured positions is given in Figure 1. As we shall mention in Appendix A, we simulate the origin of the blast waves as a sphere of high pressure and high temperature gas. In order to account for the effect of unsymmetrical source distribution in the muzzle brake, we choose different source conditions, e.g., strength and size of the sphere, for each radial line. The source conditions are adjusted so that both the calculated and the measured pressure traces are roughly matched at a single position on each line and then the calculation is checked against the other pressure traces at all other positions along that line. It should be emphasized that the actual source distribution from the muzzle brake can be obtained by solving the problem of charge detonation and the resulting barrel and muzzle flow. In a future study, we will calculate this part of flow and integrate it with the far field calculation in order to obtain a more complete and detailed picture.

The pressure traces at different distances (25', 30', 35', 40', 50', and 60') along the B-line with gun elevation at 45° are shown in Figure 2. Those in the left column are reproductions of the measured data while the results from our calculation are shown in the right column. The experimental curves show a certain amount of random oscillation whose origin is uncertain at this time. However, a discernible second peak due to wave reflection can be

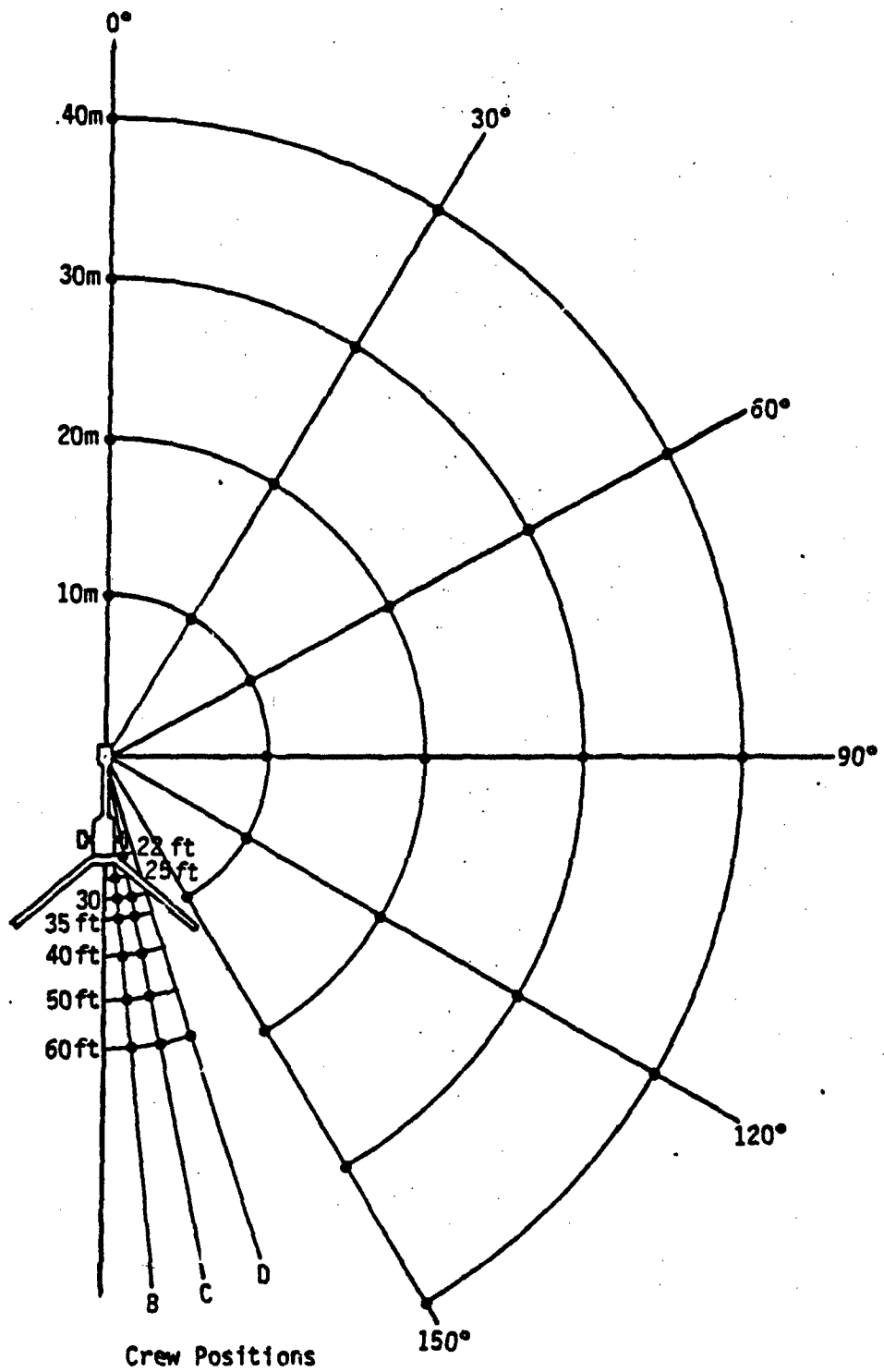


Figure 1. Ground map for locations of measurement.

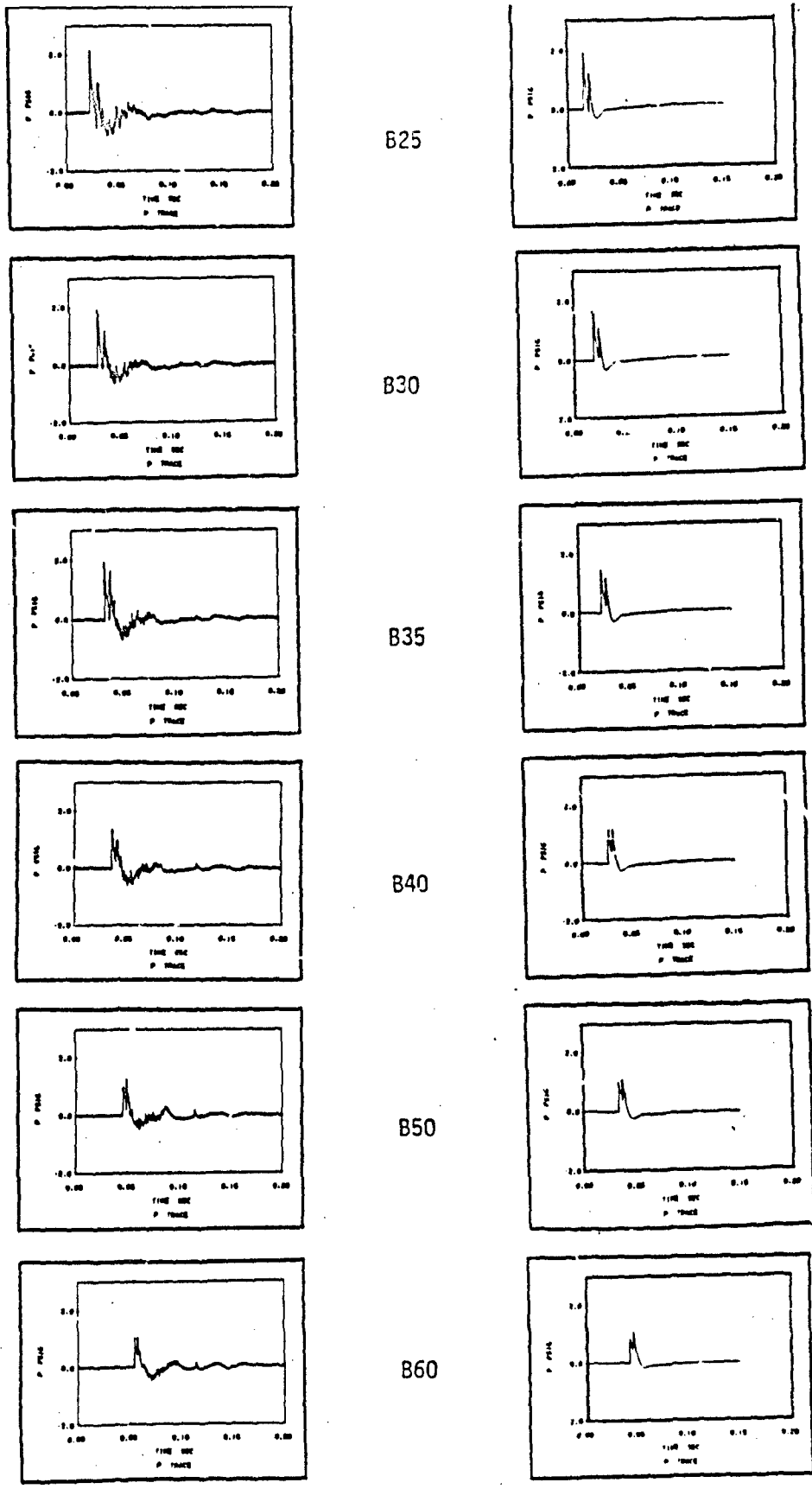


Figure 2. Measured and calculated pressure traces along B-line at 45° gun elevation

seen in all those pictures. Since the path lengths of the incident and reflected waves, as shown in Figure 42 in Appendix A, are different and their speeds of propagation are almost the same, these two waves will arrive at a certain point at different times. Both our calculation and the measurement display this effect. From a geometrical point of view, the difference of the path lengths of these two waves is longer for the points closer to the muzzle brake, as it is compared with those further away from the muzzle brake. As a consequence, the timing between the two peaks, as shown in Figures 2 and 3, is the largest at the position with distance of 25' while it is the smallest at 60'. Due to the longer path length of the reflected wave than that of the incident wave, its strength should be weaker than that of the incident one. A question may arise as to why the second peak has a larger amplitude than the first one for some cases, for instance, 50' and 60'. This can be explained as due to the overlapping of the resident times for both waves, their amplitudes are superimposed to attain such a value, exceeding that of the first one. Generally, our calculation has been quite successful in capturing the structure of the compression part of the wave. As shown in Figure 3, good agreement can be seen among the calculated and measured quantities, e.g., the amplitude of the incident wave p_1 , the ratio of the amplitudes of the second peak to the first one p_2/p_1 , and the timing between the two peaks Δt . Nevertheless, the rarefaction part of the wave in our calculation is narrower in time and shallower in amplitude than that of the measured one. This discrepancy is probably due to our inexact treatment of the time dependent boundary condition at the muzzle brake, which can only be obtained after the abovementioned problem of charge detonation and its resulting barrel flow is solved.

Figures 4 and 5 show the lung response, in terms of lung pressure and its change in gaseous volume, on the crew positions along the B-line at 45° gun elevation. Those in the left column are the results from the lung simulation with the measured overpressure as its driving force while those using our calculated overpressure as driving forces are shown in the right column. Very good agreement can be seen again in the compression part. In response to the random oscillation associated with the measured pressure traces, as mentioned above, the corresponding lung pressure and its change of gaseous volume show wiggles in both the expansion and tail regions. On the other hand, a regular

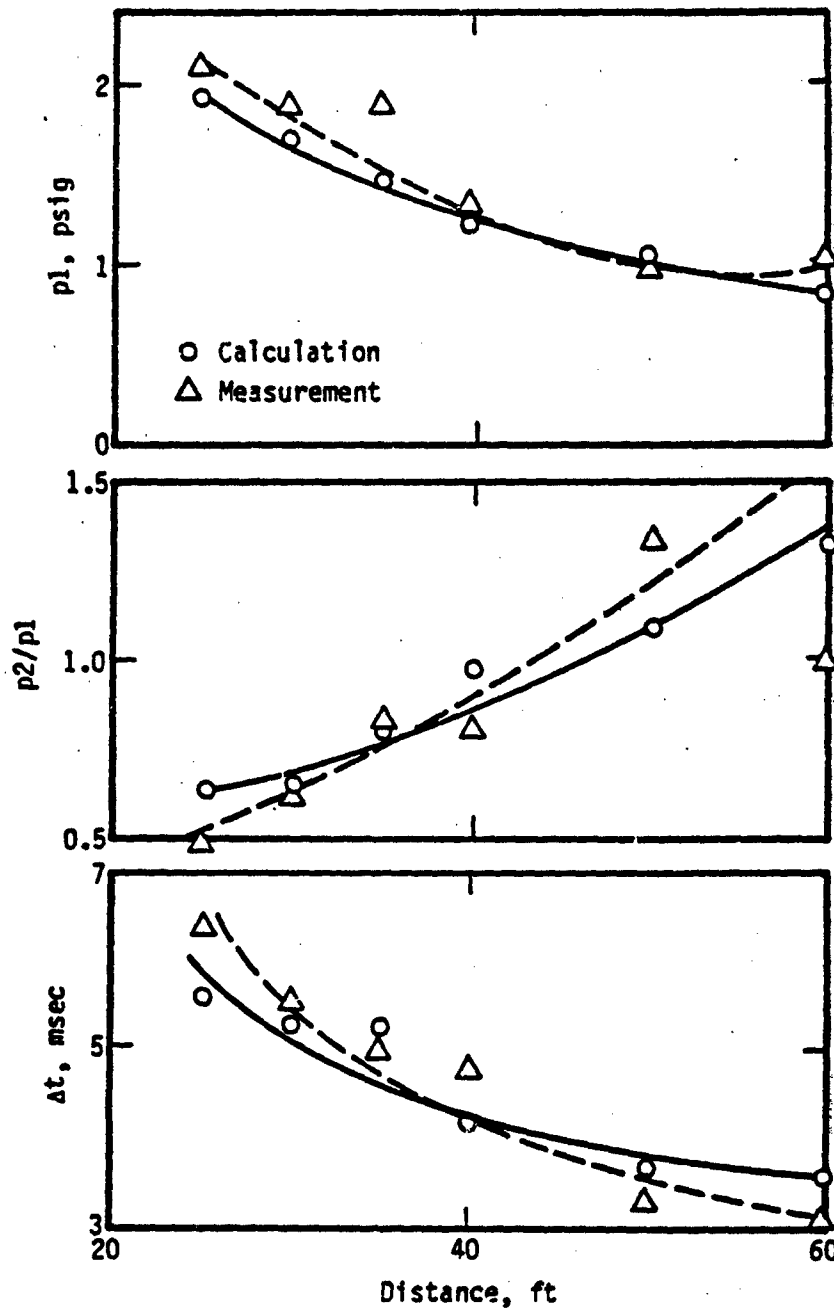
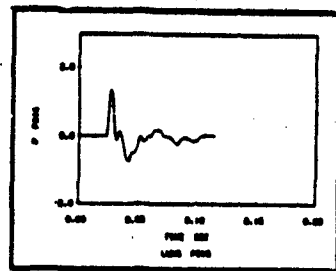
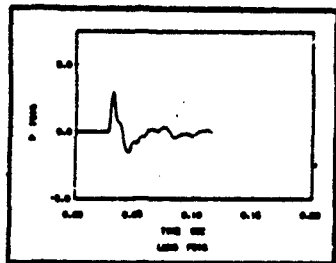
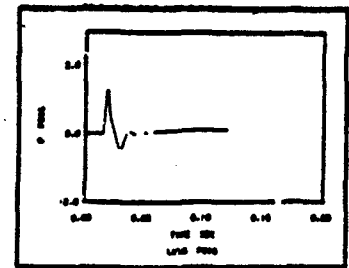


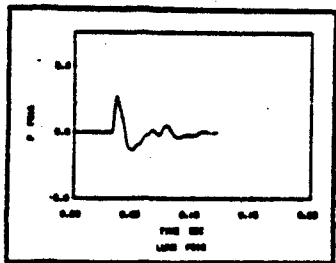
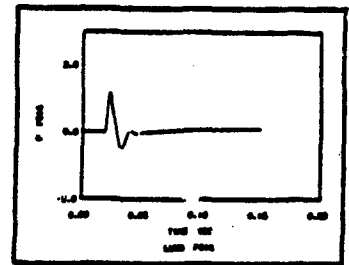
Figure 3. Variation of p_1 , p_2/p_1 and Δt with distance along B-line with 45° gun elevation



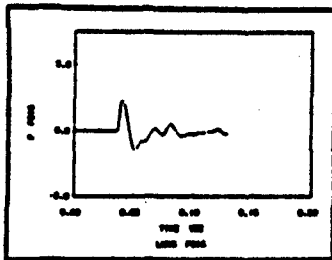
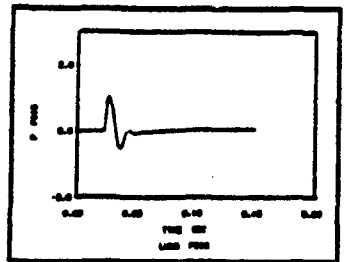
B25



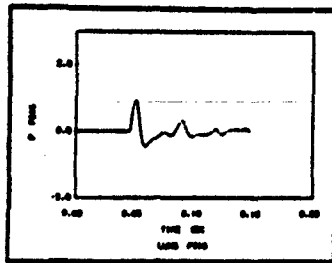
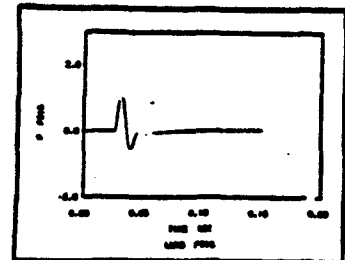
B30



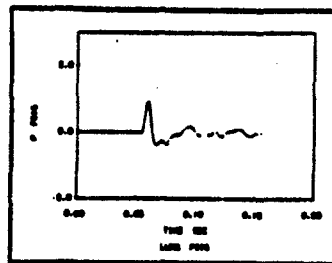
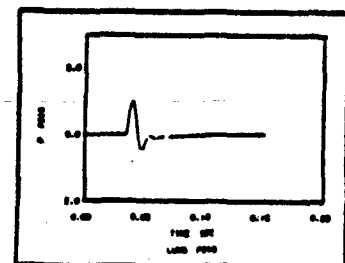
B35



B40



B50



B60

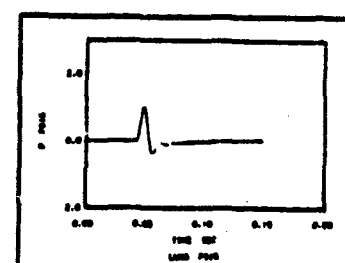


Figure 4. Lung pressure traces based on measured and calculated blast pressures along B-line at 45° gun elevation

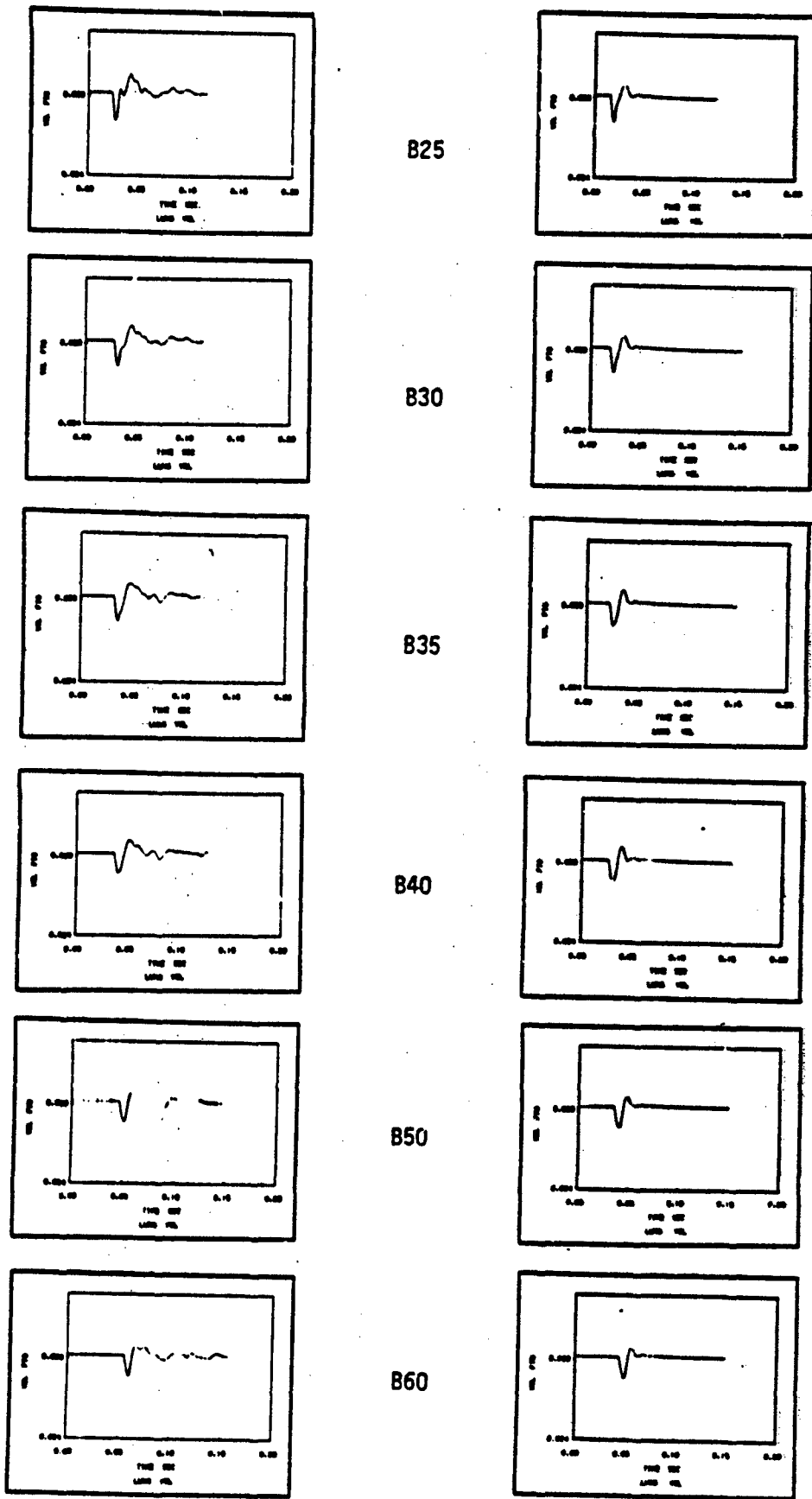
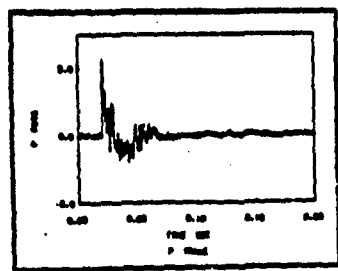


Figure 5. Change of gaseous volume of lung based on measured and calculated blast pressures along B-line at 45° gun elevation

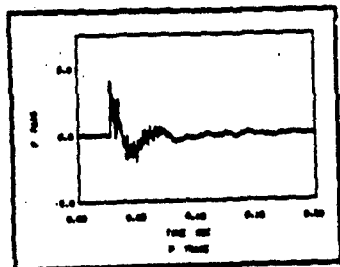
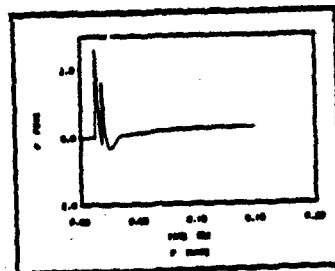
underdamping in the tail region can be seen in the counterparts with our calculated pressure traces as the driving forces. It should be noted that the validity of the lung model is established based on the sound comparison between numerical simulation and experiments on animals [Reference 1]. Since there is no experiment on human beings to our knowledge, it seems logical to assume the validity of this model can be extended to study the response on human lung. In light of this, let us suppose those in the left column are the true human lung response to the real blast overpressure, then our calculation, as shown in the right column, indeed predicts the right trend.

Figures 6 and 7 show the pressure traces, p_1 , p_2/p_1 and Δt along the C-line at 45° gun elevation. Figures 8 and 9 show the corresponding lung pressure and change in gaseous volume. Good agreement can be seen again. The reproducibility of the measured data and its corresponding lung response on crew position at C22 with 45° gun elevation is shown in Figure 10 for four different shots. The general structure of these curves is well preserved, except no distinguishable second peak can be seen in the pressure trace for Shot No. 2. Moreover, Figure 11 shows very close agreement between the measured and calculated pressure traces and their corresponding lung responses on crew position at D60 with 45° gun elevation.

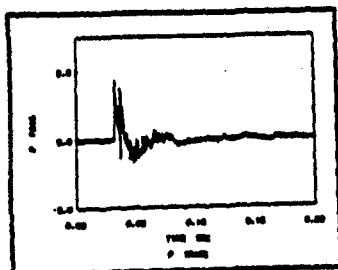
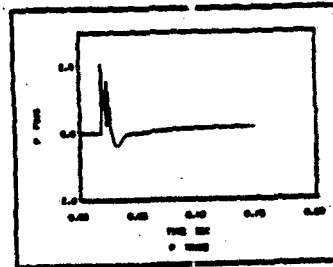
The same sequence of comparison from Figures 2 to 11 for 45° gun elevations, as mentioned above, is repeated for 15° and is shown in Figures 12 to 21. In view of the gun geometry, the difference of the path lengths between the incident and reflected waves is shorter for modest gun elevation, as it is compared with that of higher elevation. Consequently, the timings between two peaks are shorter for 15° gun elevation than those with 45° (see Figures 13 and 17 versus Figures 3 and 7 for comparison). It is the same reason, together with the argument of the overlapping of the resident times of the two waves, that explains why the second peak overtakes the first one for positions closer to the muzzle brake at modest gun elevation. Again, Figure 20 shows the reproducibility of the measured data and its corresponding lung response at C22 with 15° gun elevation for four different shots. These curves look very similar with an exception that the pressure trace in Shot No. 23 has smaller second peak while the other three cases do not.



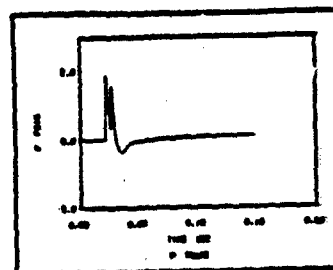
C22



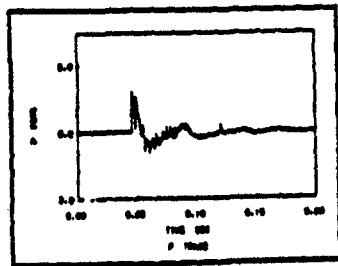
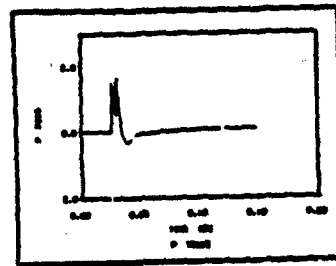
C30



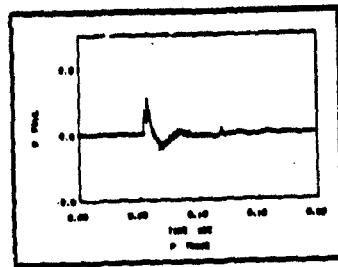
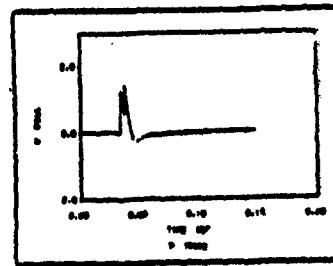
C35



C40



C50



C60

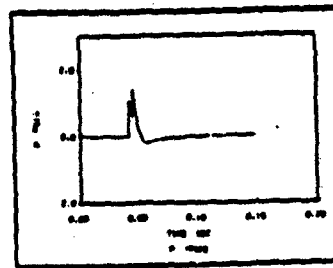


Figure 6. Measured and calculated pressure traces along C-line at 45° gun elevation

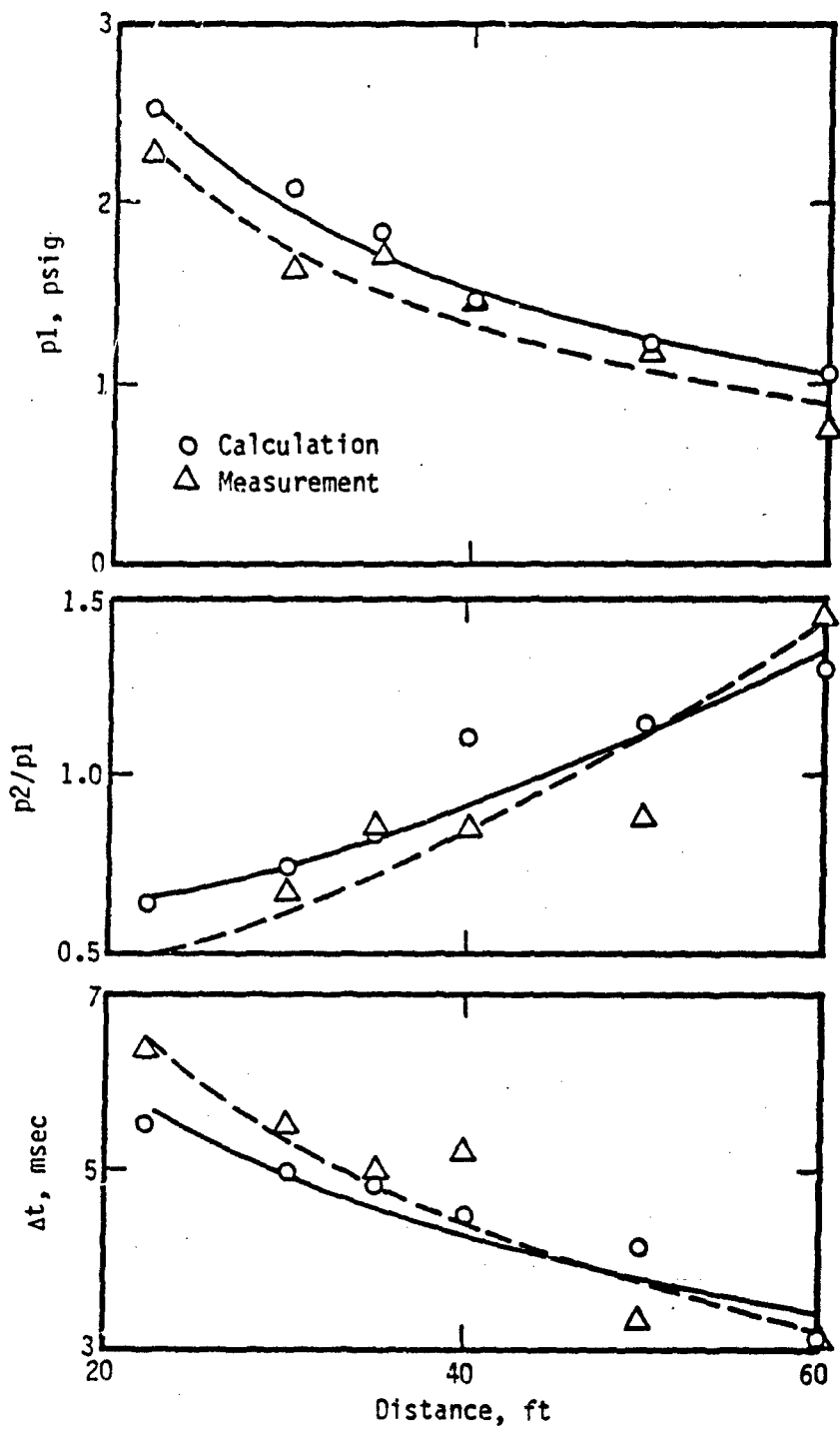
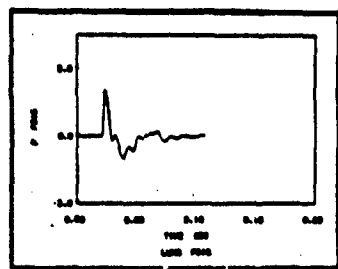
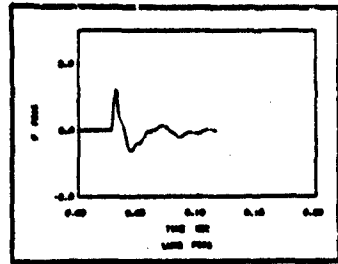
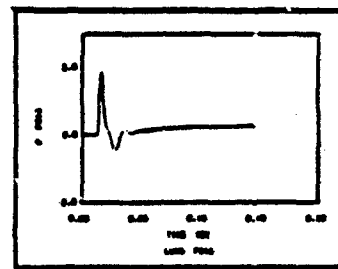


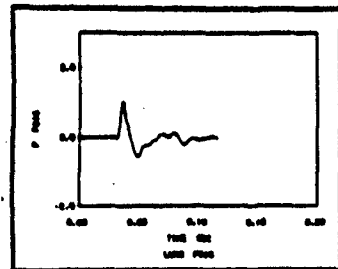
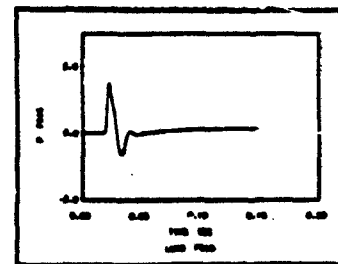
Figure 7. Variation of p_1 , p_2/p_1 and Δt with distance along C-line with 45° gun elevation



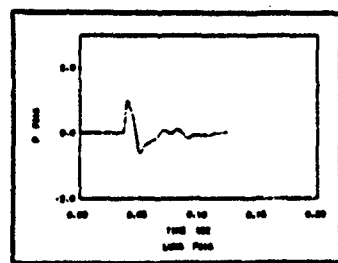
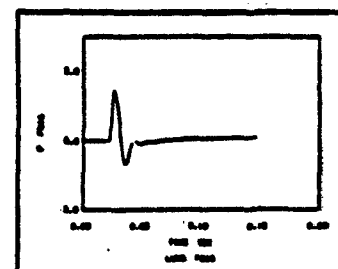
C22



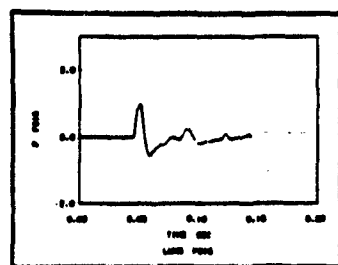
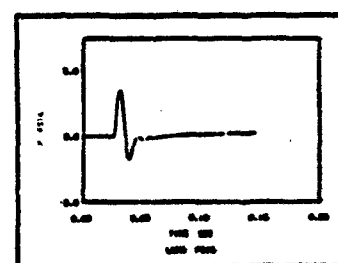
C30



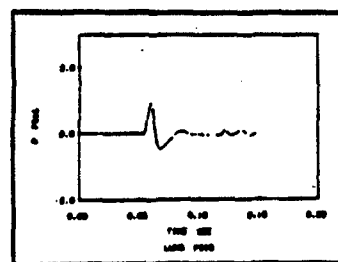
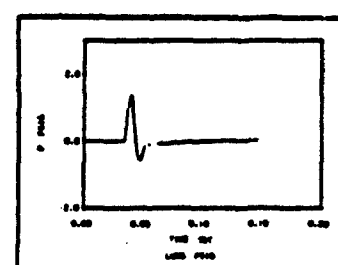
C35



C40



C50



C60

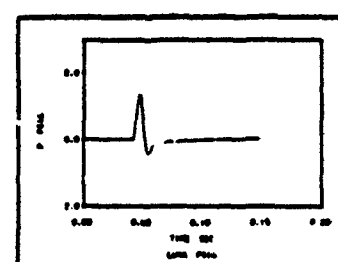
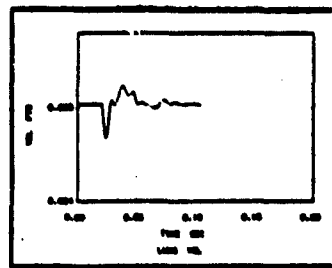
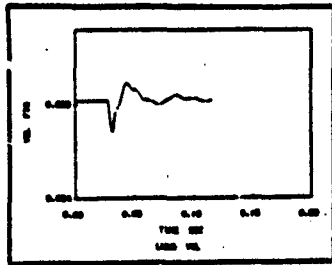
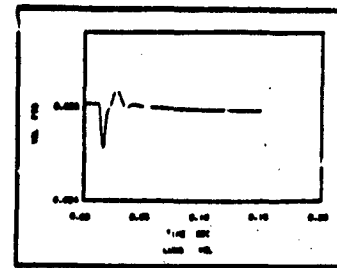


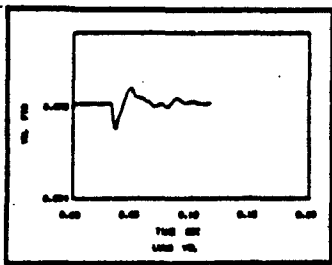
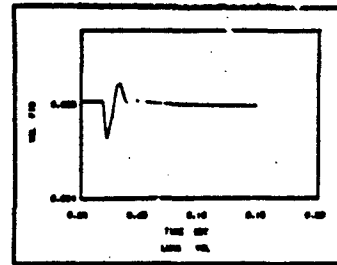
Figure 8. Lung pressure traces based on measured and calculated blast pressures along C-line at 45° gun elevation



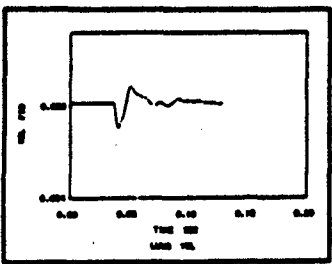
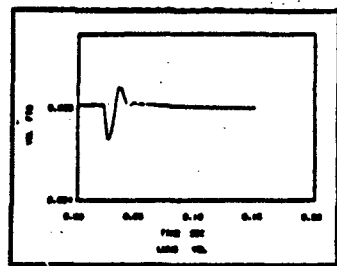
C22



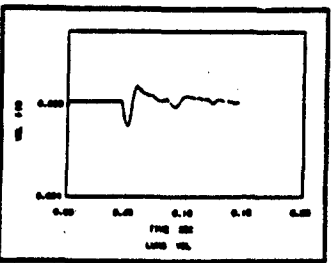
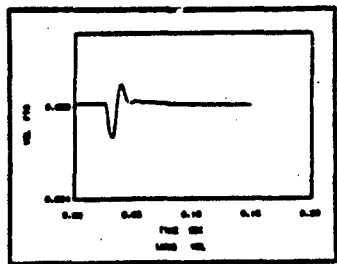
C30



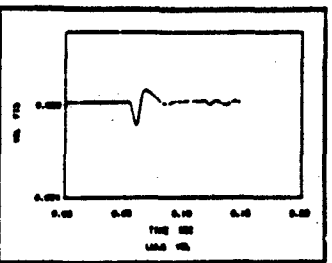
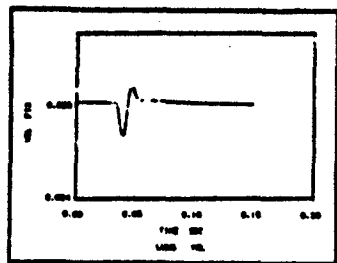
C35



C40



C50



C60

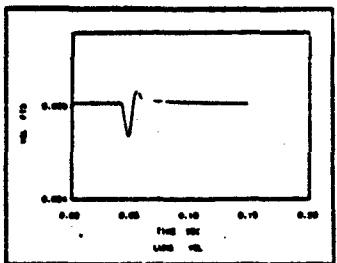
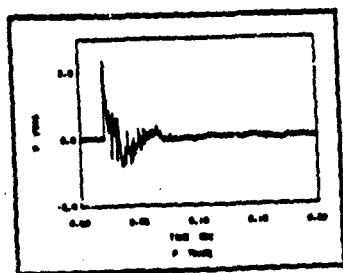
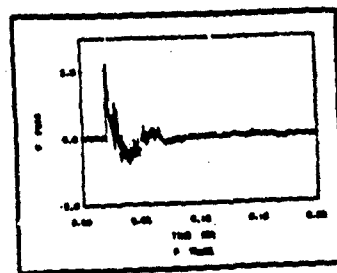


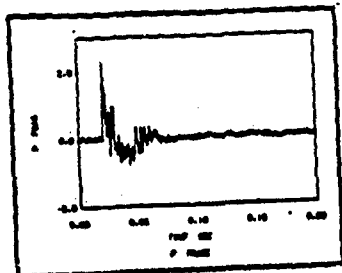
Figure 9. Change of gaseous volume of lung based on measured and calculated blast pressures along C-line at 45° gun elevation



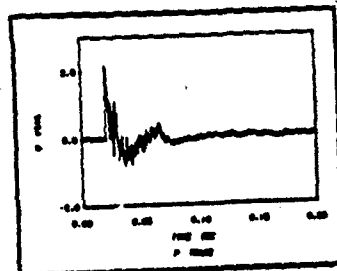
Shot #2



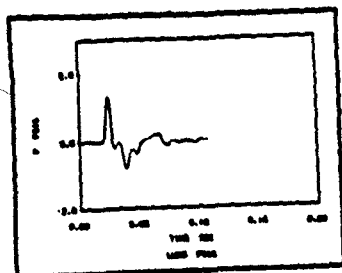
Shot #11



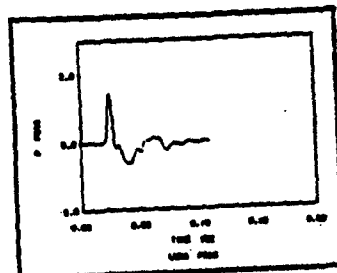
Shot #20



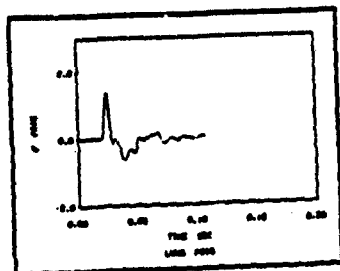
Shot #29



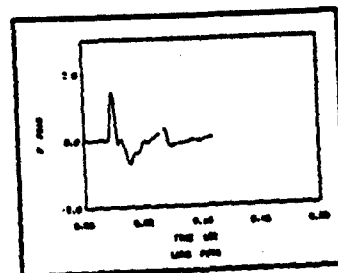
Shot #2



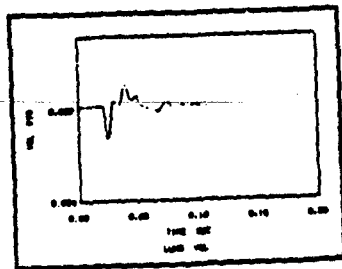
Shot #11



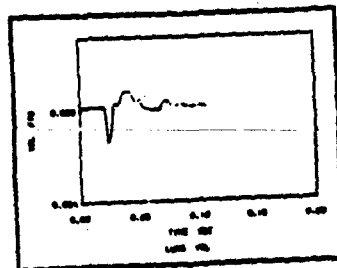
Shot #20



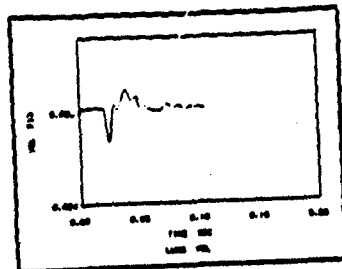
Shot #29



Shot #2



Shot #11



Shot #20



Shot #29

Figure 10. Measured pressure traces and their resulting lung pressures and changes of lung volume at C22 with 45° gun elevation

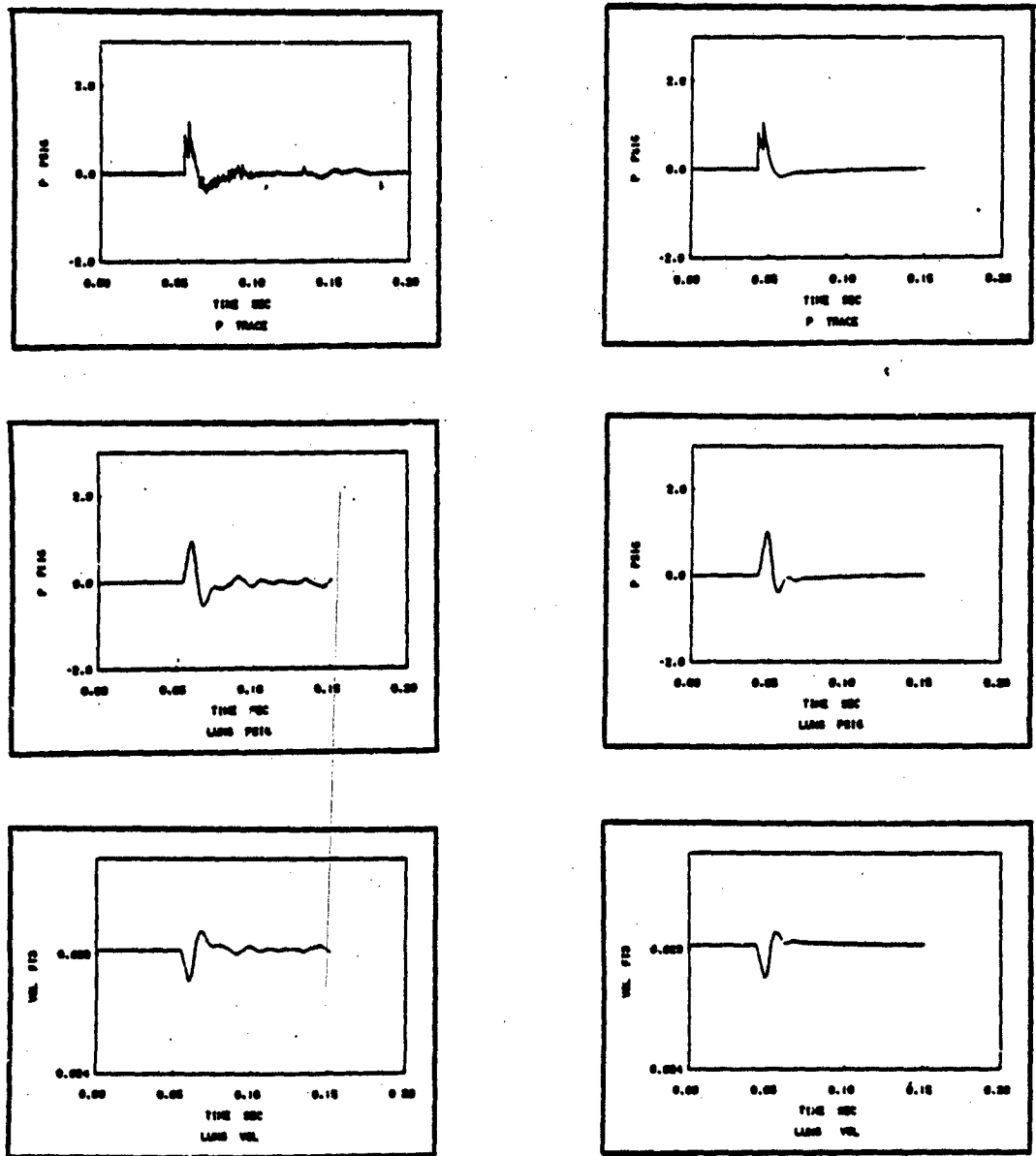


Figure 11. Measured and calculated pressure traces and their resulting lung pressures and changes of lung volume at D60 with 45° gun elevation

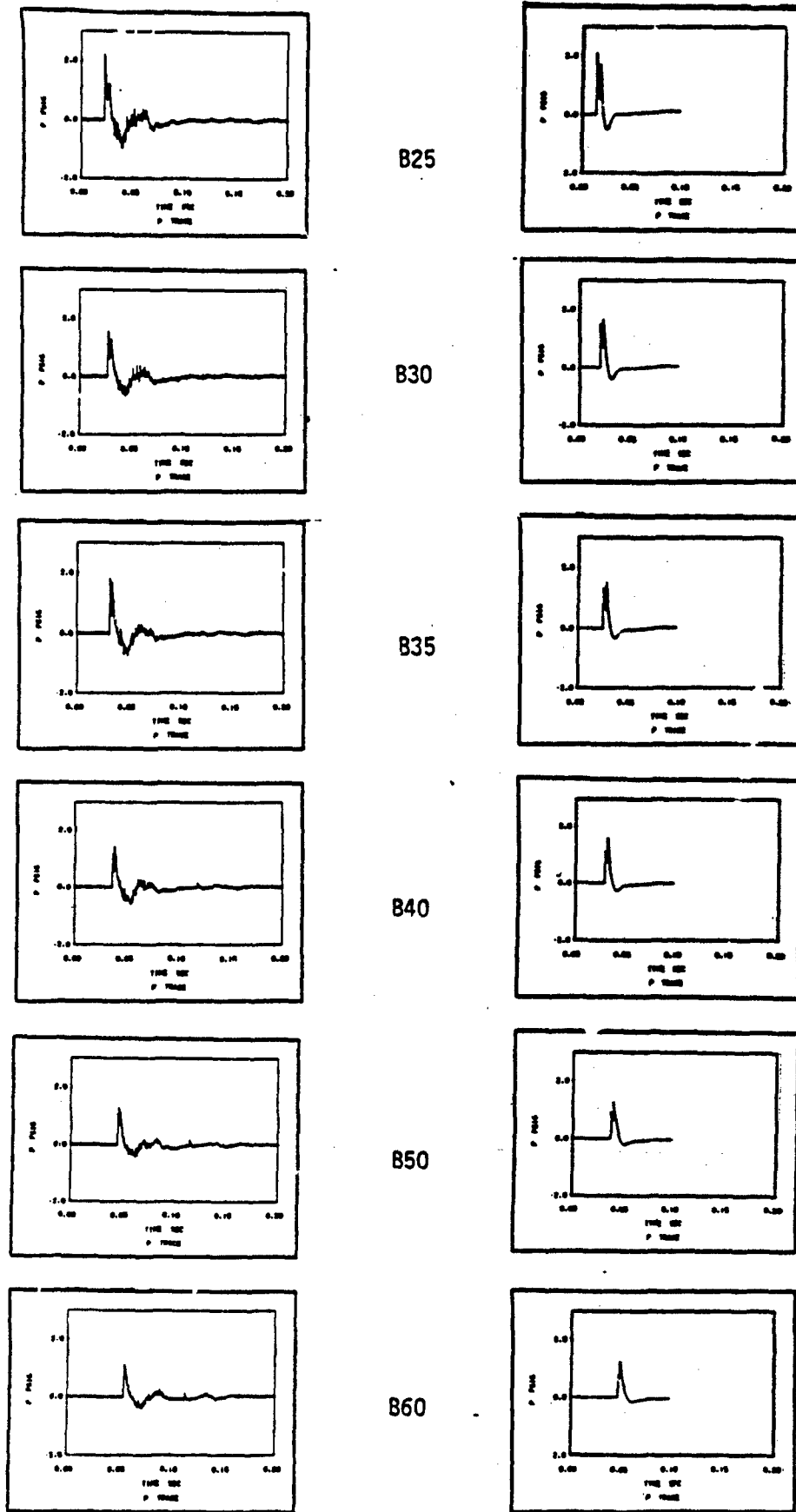


Figure 12. Measured and calculated pressure traces along B-line at 15° gun elevation

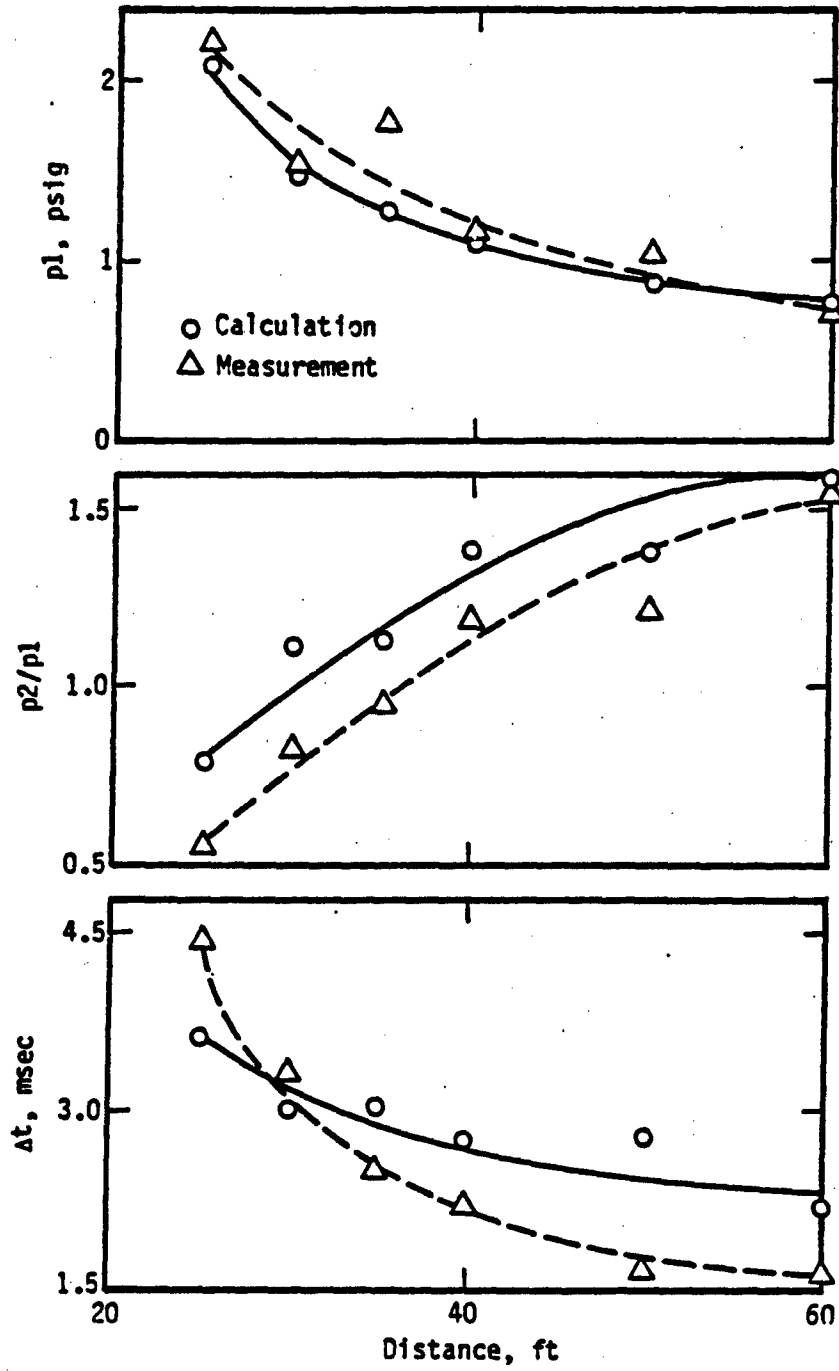
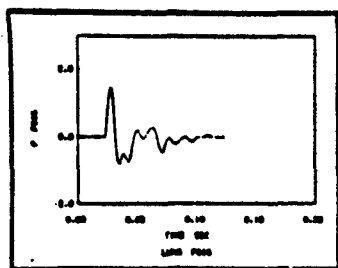
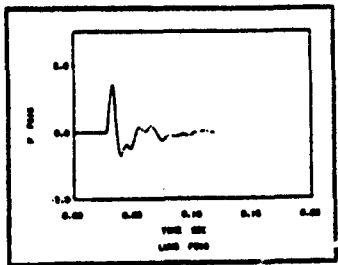
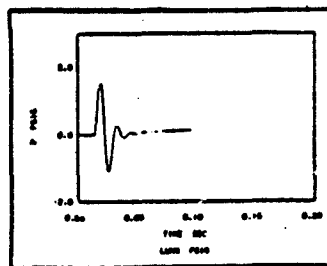


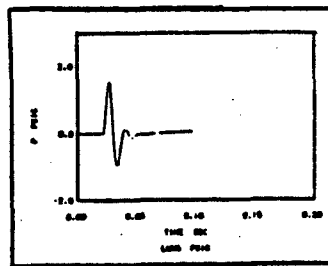
Figure 13. Variation of p_1 , p_2/p_1 and A_t with distance along B-line with 15° gun elevation



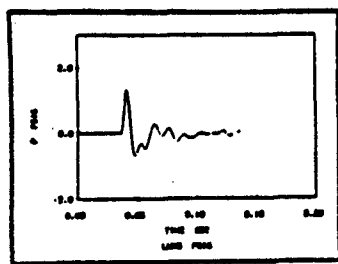
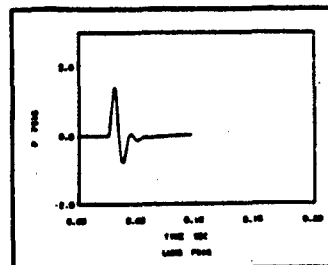
B25



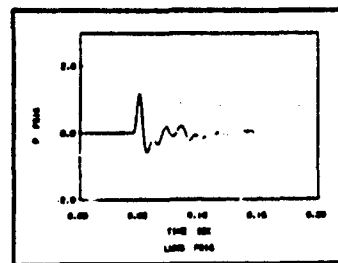
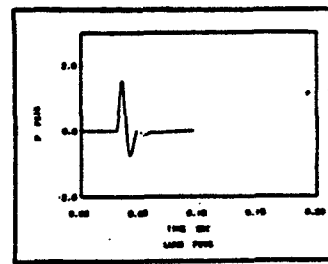
B30



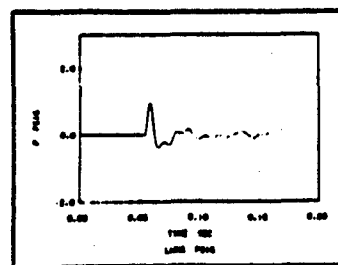
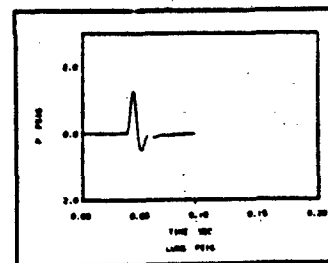
B35



B40



B50



B60

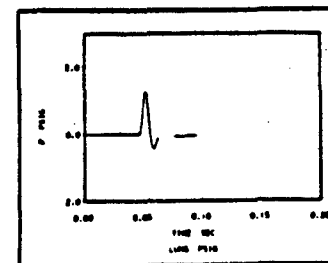


Figure 14. Lung pressure traces based on measured and calculated blast pressures along B-line at 15° gun elevation

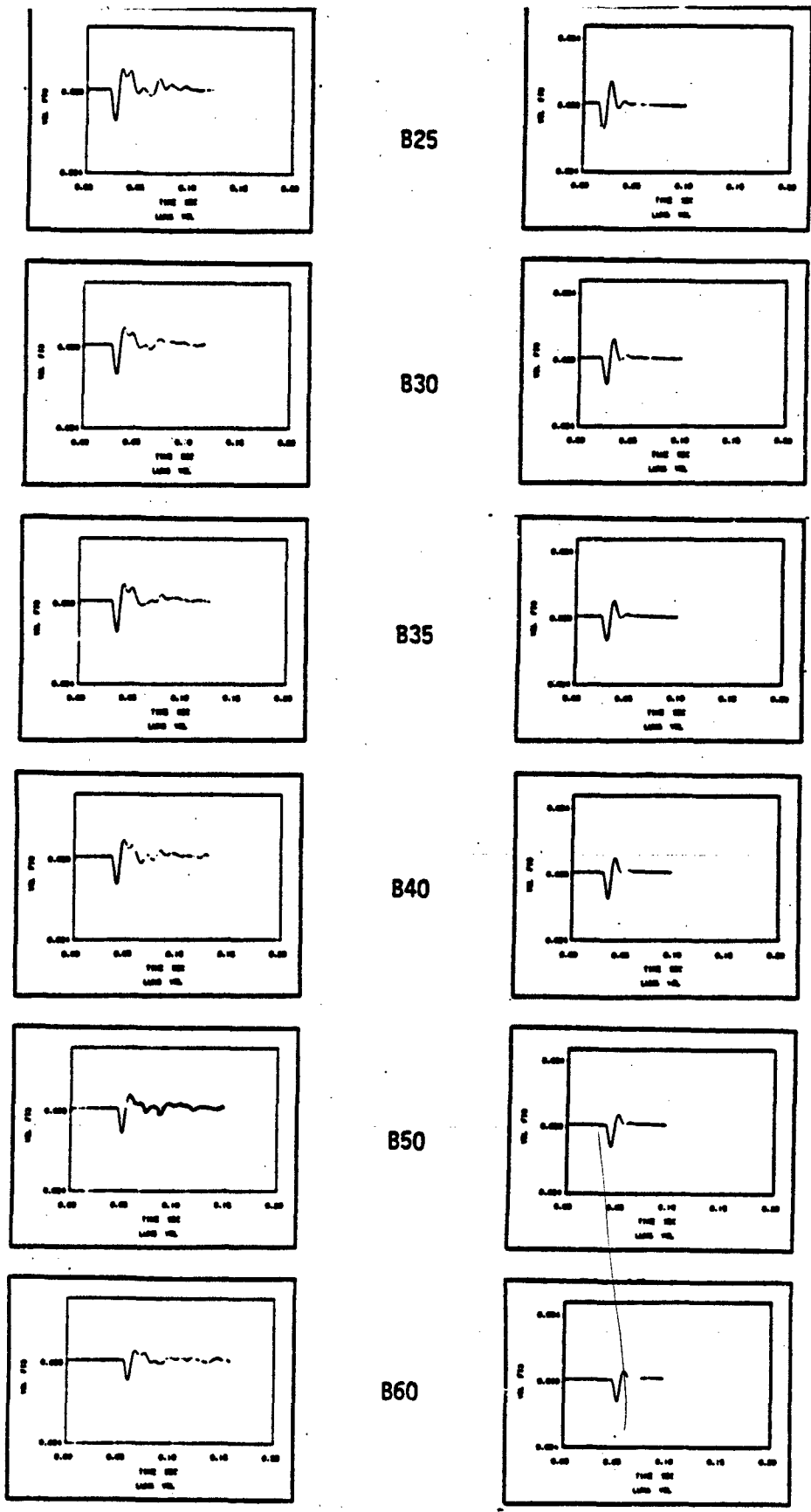


Figure 15. Change of gaseous volume of lung based on measured and calculated blast pressures along B-line at 15° gun elevation

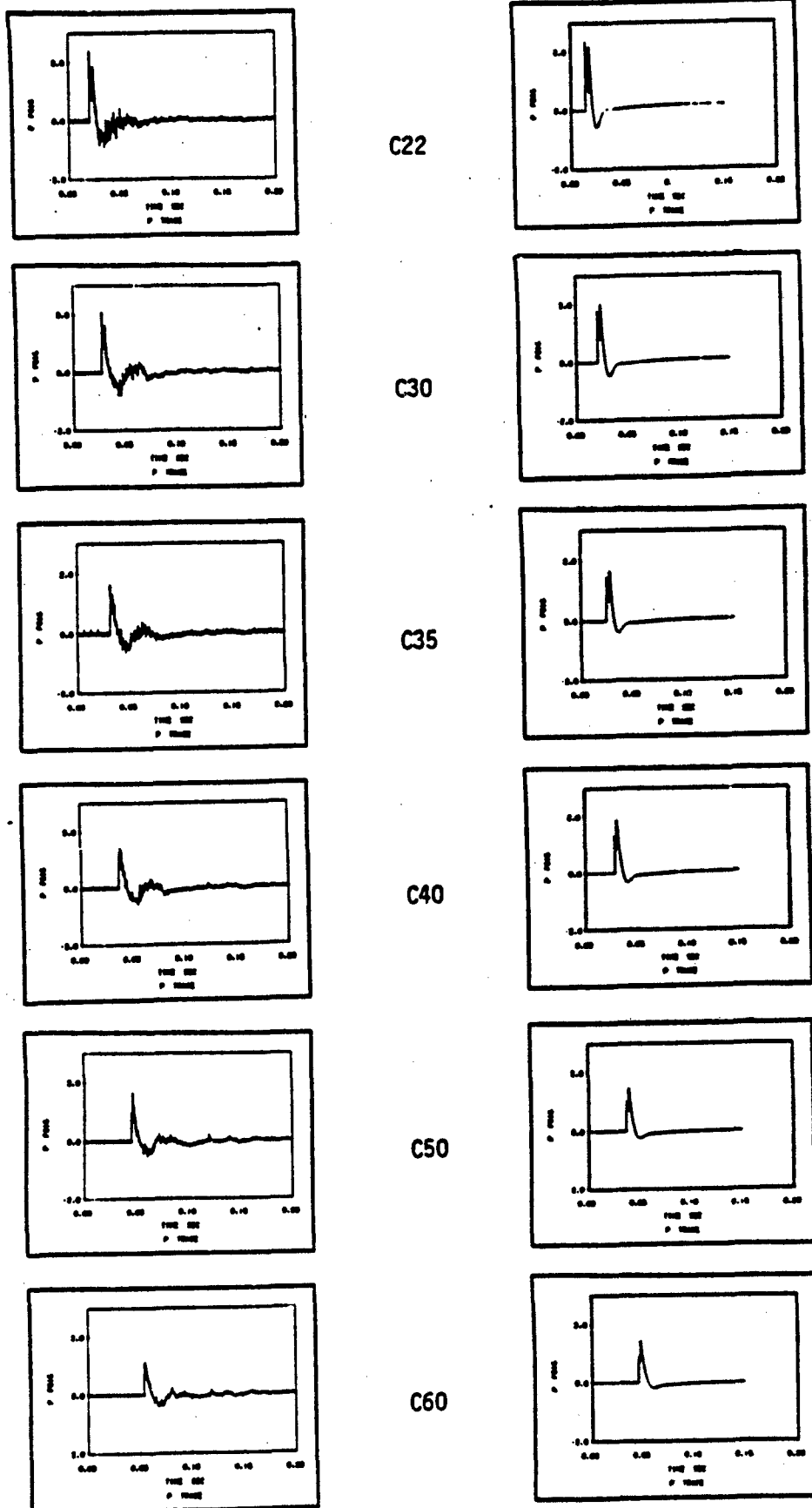


Figure 16. Measured and calculated pressure traces along C-line at 15° gun elevation

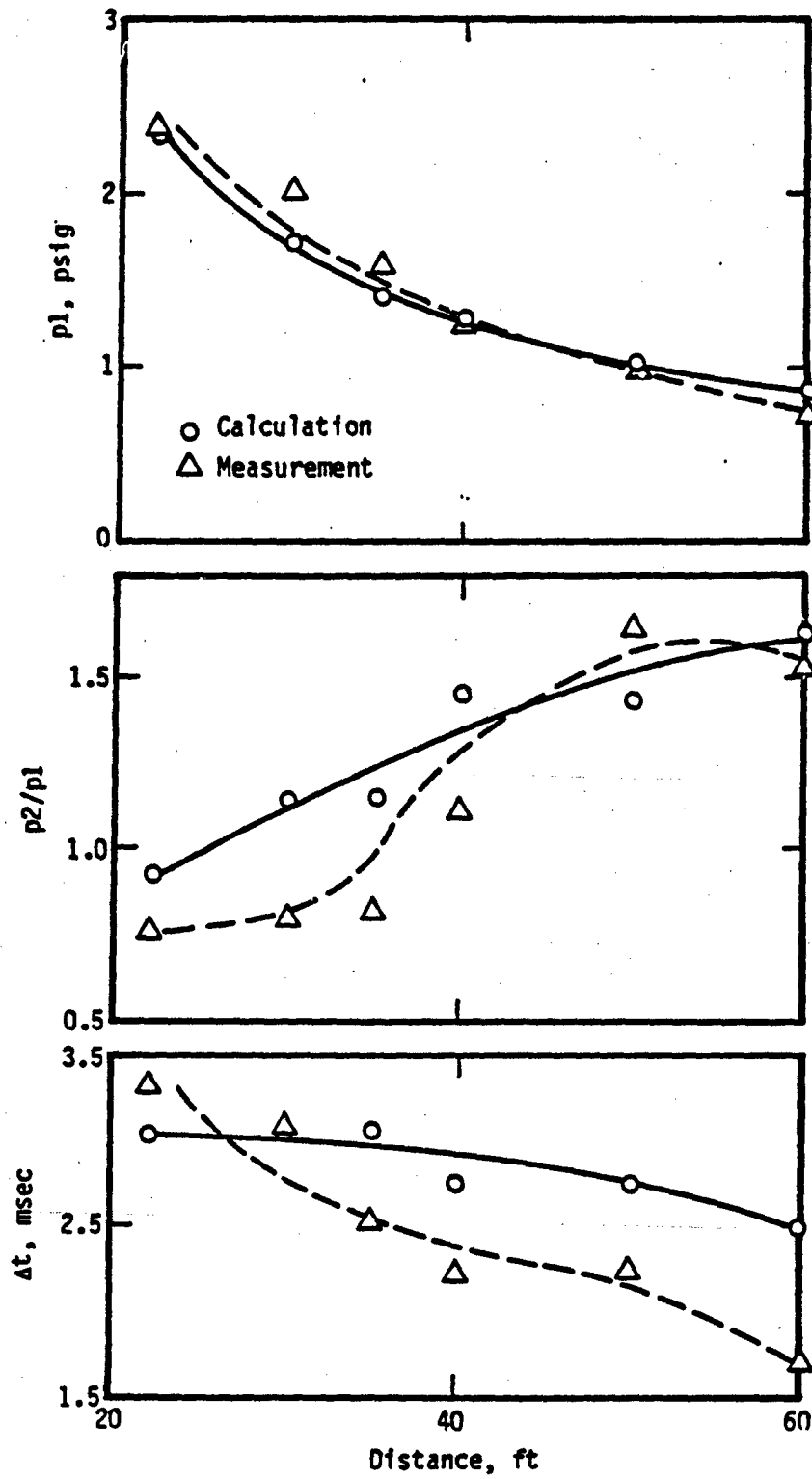
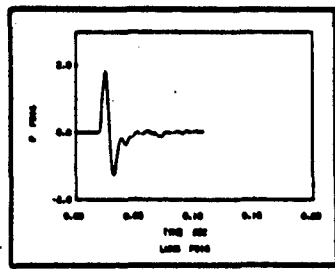
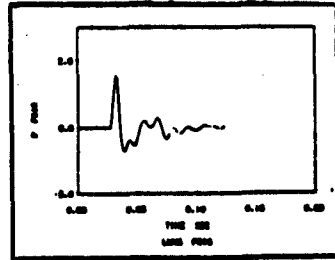
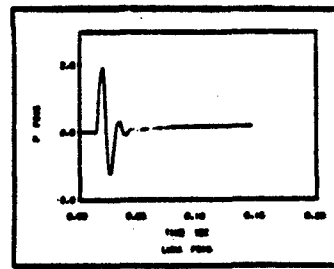


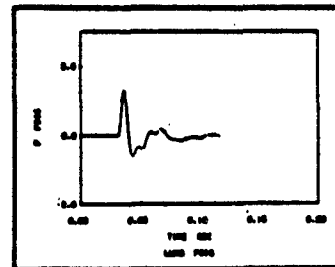
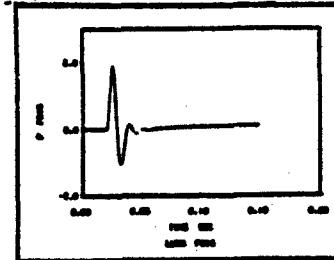
Figure 17. Variation of p_1 , p_2/p_1 and Δt with distance along C-1 line with 15° gun elevation



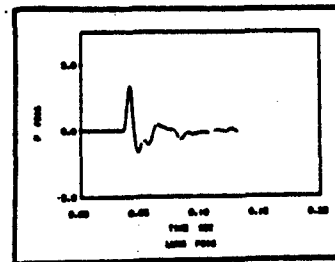
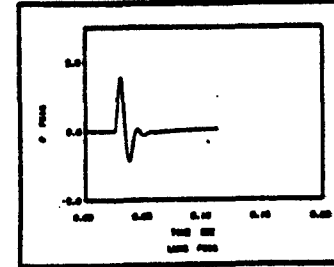
C22



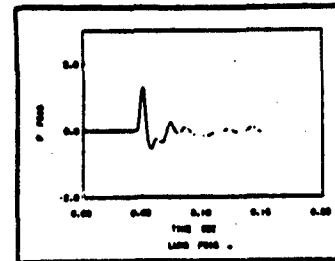
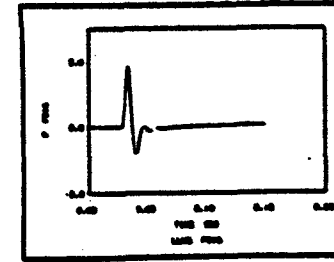
C30



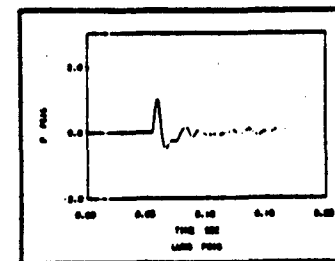
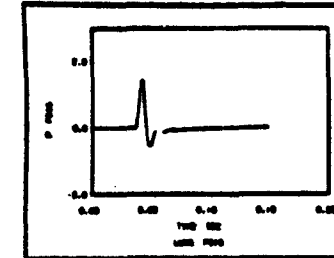
C35



C40



C50



C60

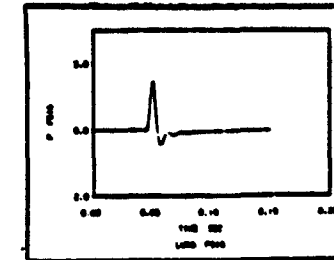


Figure 18. Lung pressure traces based on measured and calculated blast pressures along C-line at 15° gun elevation

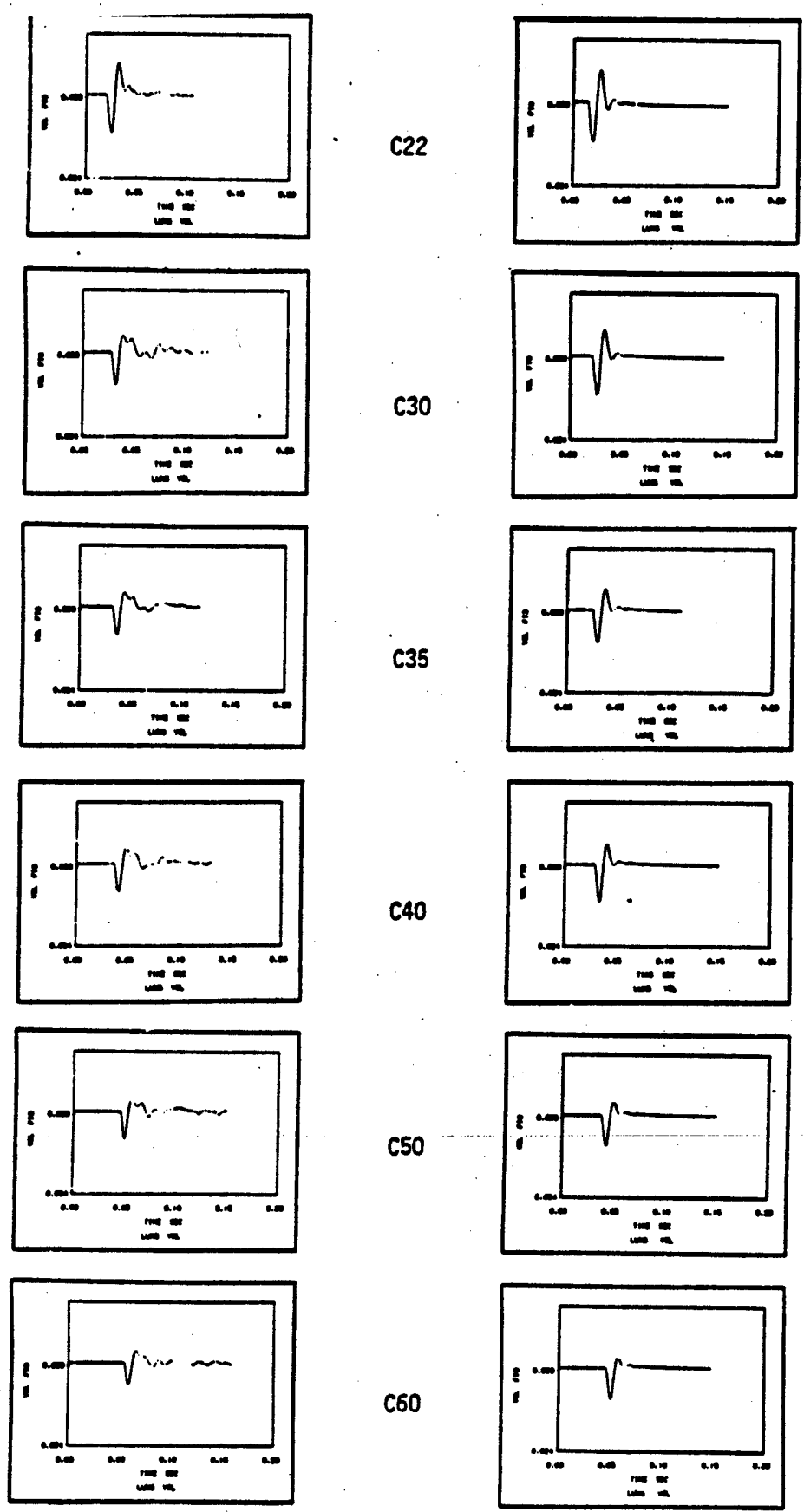


Figure 19. Change of gaseous volume of lung based on measured and calculated blast pressures along C-line at 15° gun elevation

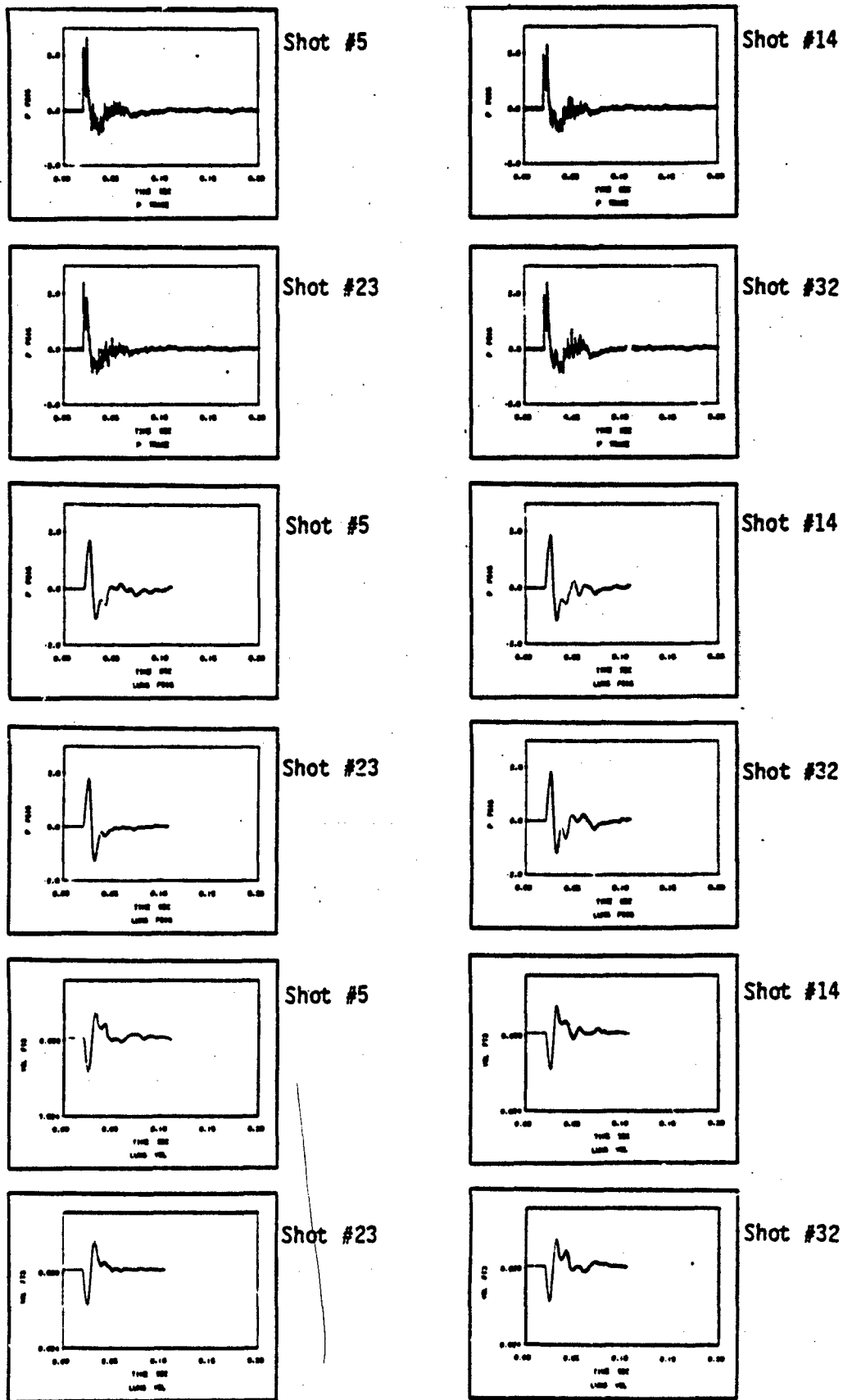


Figure 20. Measured pressure traces and their resulting lung pressures and changes of lung volume at C22 with 15° gun elevation

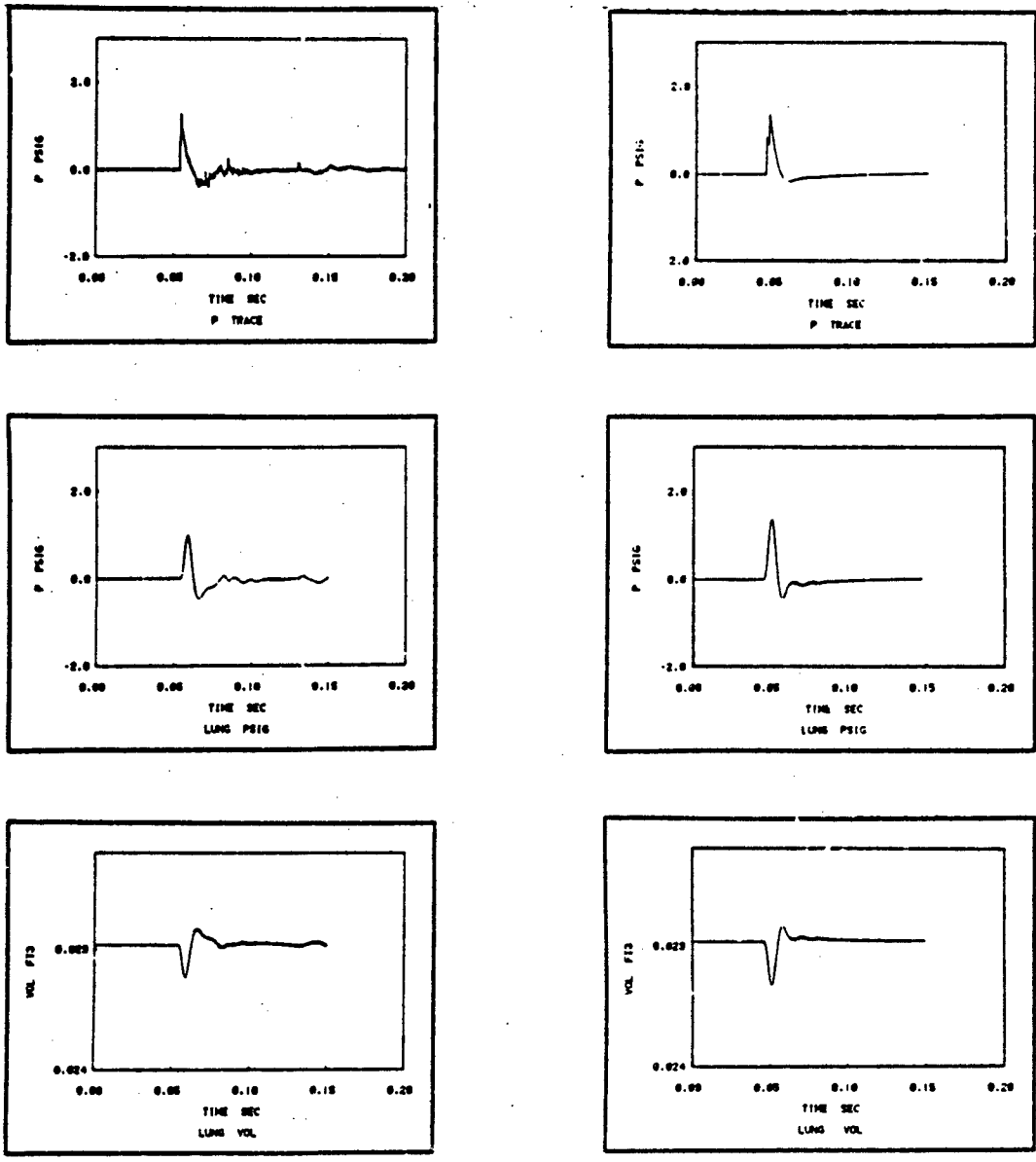
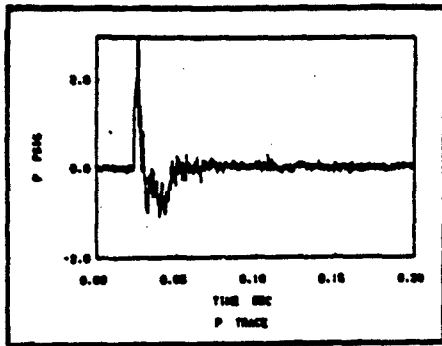


Figure 21. Measured and calculated pressure traces and their resulting lung pressures and changes of lung volume at D60 with 15° g/n elevation

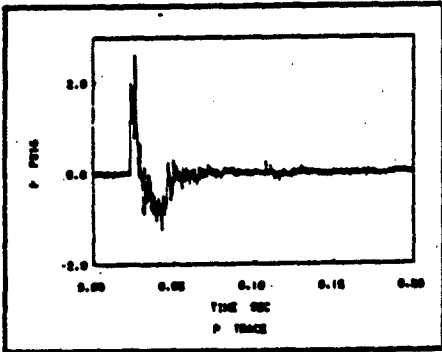
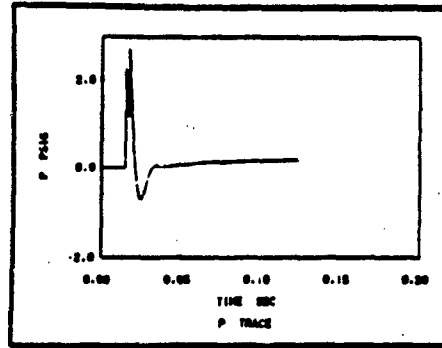
So far we have shown in the crew positions (5' height) various effects on pressure traces and their corresponding lung responses, namely, the variation of the distance away from the muzzle brake, the angular variation of the measured positions, and the variation of the gun elevation. In order to complete the study at the crew positions, we include the effect of the variation of the height of the measured positions. Figures 22 and 23 show the pressure traces, p_1 , p_2/p_1 and Δt at different heights (3', 4', 5', and 6') at C22 with 15° gun elevation. Good correlation among measurement and calculation can again be observed. Since the difference of the path lengths between the incident and reflected waves is shorter for the points closer to the ground, the timing between the two peaks, as shown in Figure 23, is the smallest at the position with 3' height while it is the largest at 6'.

Figures 24 to 35 show the pressure traces, p_1 , p_2/p_1 and Δt at different distances (10 m, 20 m, 30 m and 40 m) along the 0°, 30°, 60°, 90°, 120° and 150° lines at 45° gun elevation. In these figures, a distinguishing feature is shown, namely, the rarefaction part of the wave is flattened out as it moves further away from the muzzle brake. The reason is probably that at large distances the wave front has a smaller curvature and behaves more like a plane wave. Theoretically, the plane wave consists only of either a compression pulse or a rarefaction pulse. Therefore, the waveform at points very far from the muzzle brake, resembles the plane wave rather than the spherical wave. Furthermore, the timing between the two peaks of the pressure traces becomes less distinguishable for points further away from the muzzle brake since the path lengths of both the incident and reflected waves are almost identical at those points.

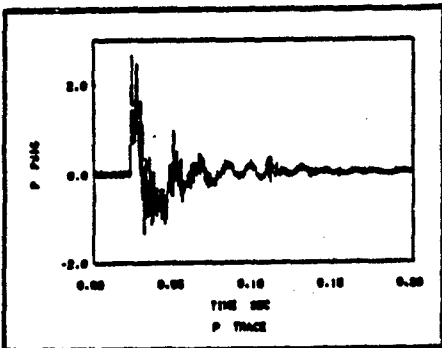
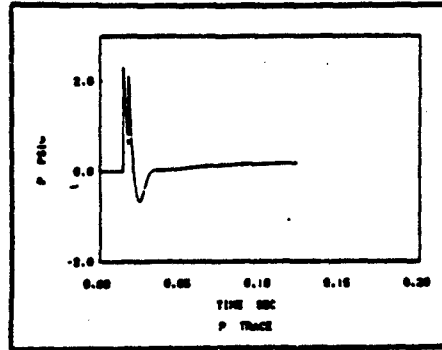
Finally, Figure 36 shows the comparison of the calculated and measured amplitude of the incident wave, i.e., the first peak in the pressure trace, in the whole field at 45° gun elevation. Both results indicate that the source distribution in the muzzle brake is stronger near 0° and also in the range from 60° to 120°, which is consistent with the geometrical configuration of the muzzle brake.



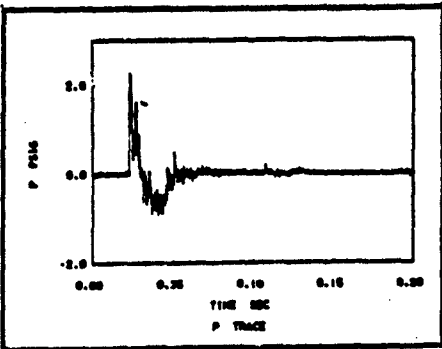
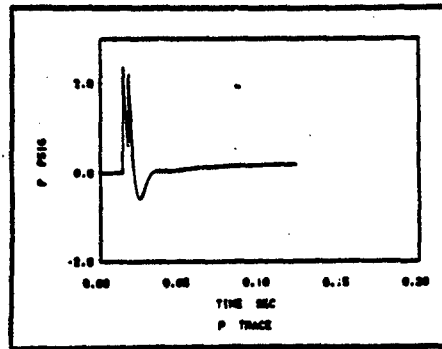
3-



4-



5-



6-

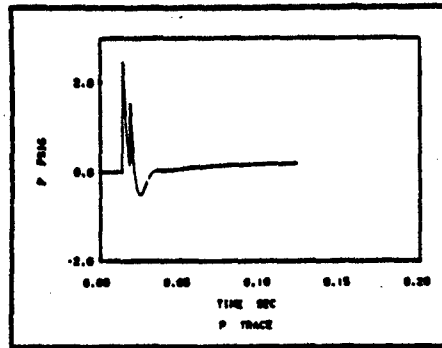


Figure 22. Measured and calculated pressure traces at C22 with 15° gun elevation

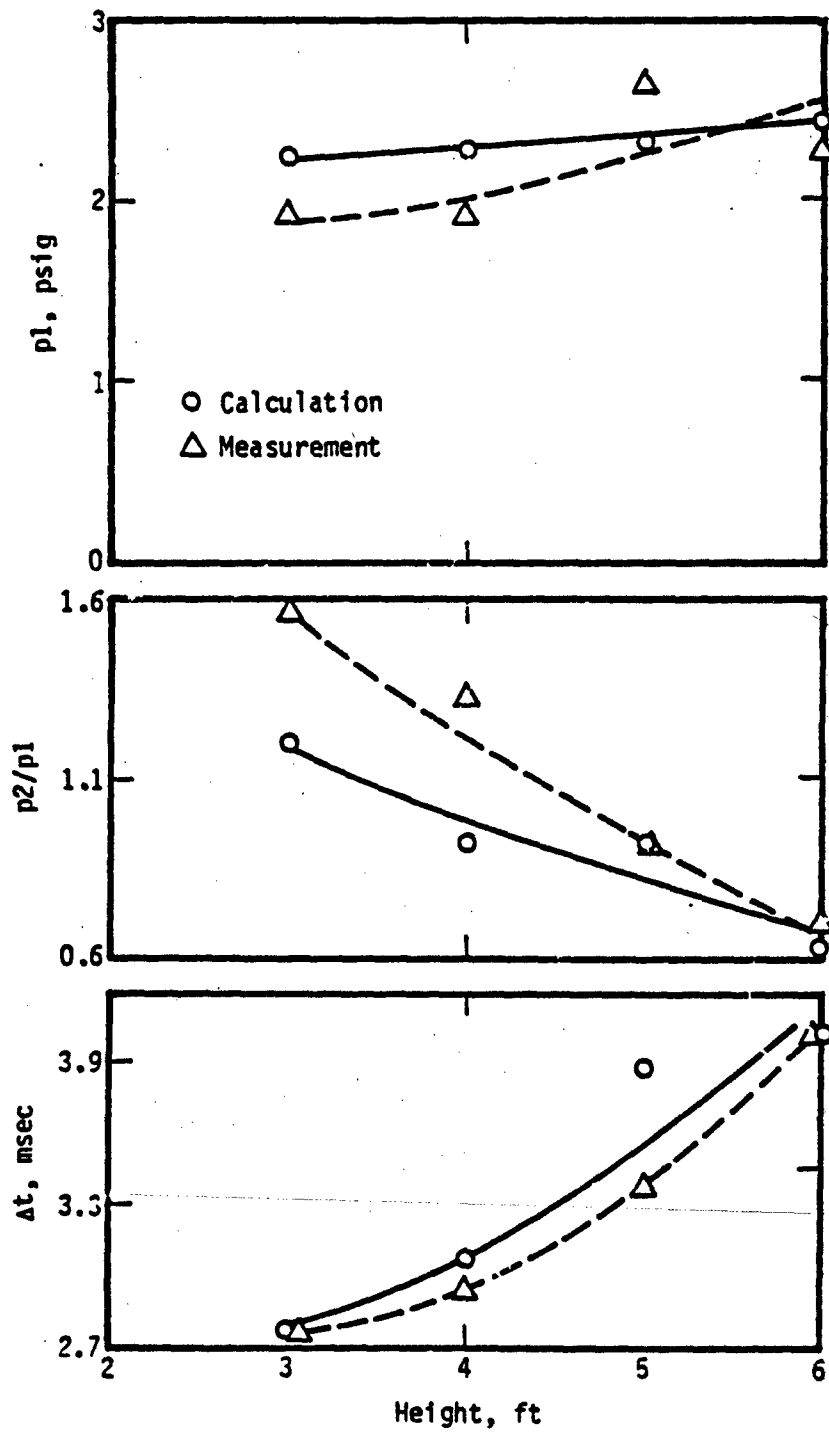


Figure 23. Variation of p_1 , p_2/p_1 and Δt with height at C22 with 15° gun elevation

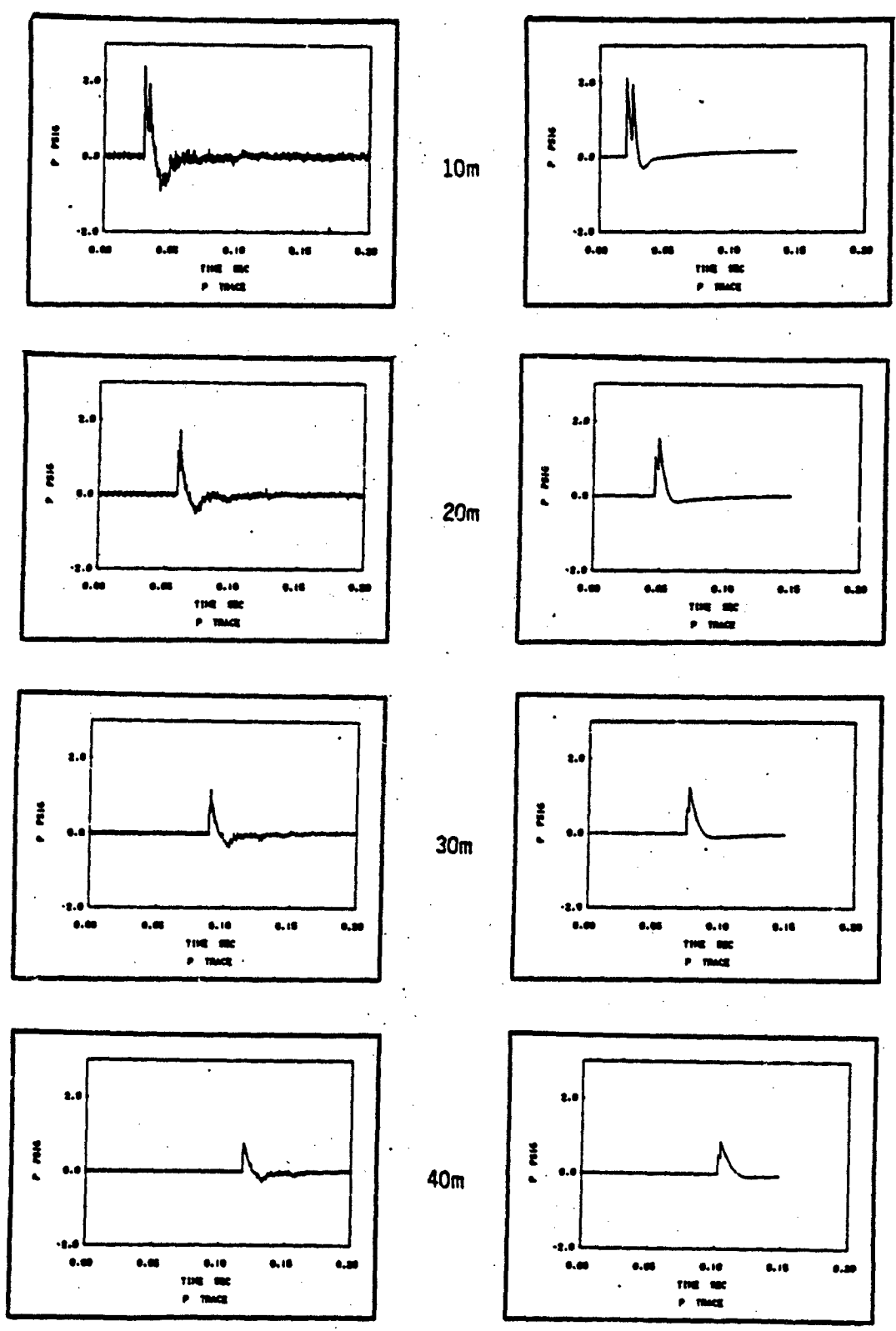


Figure 24. Measured and calculated pressure traces along 0°-line at 45° gun elevation

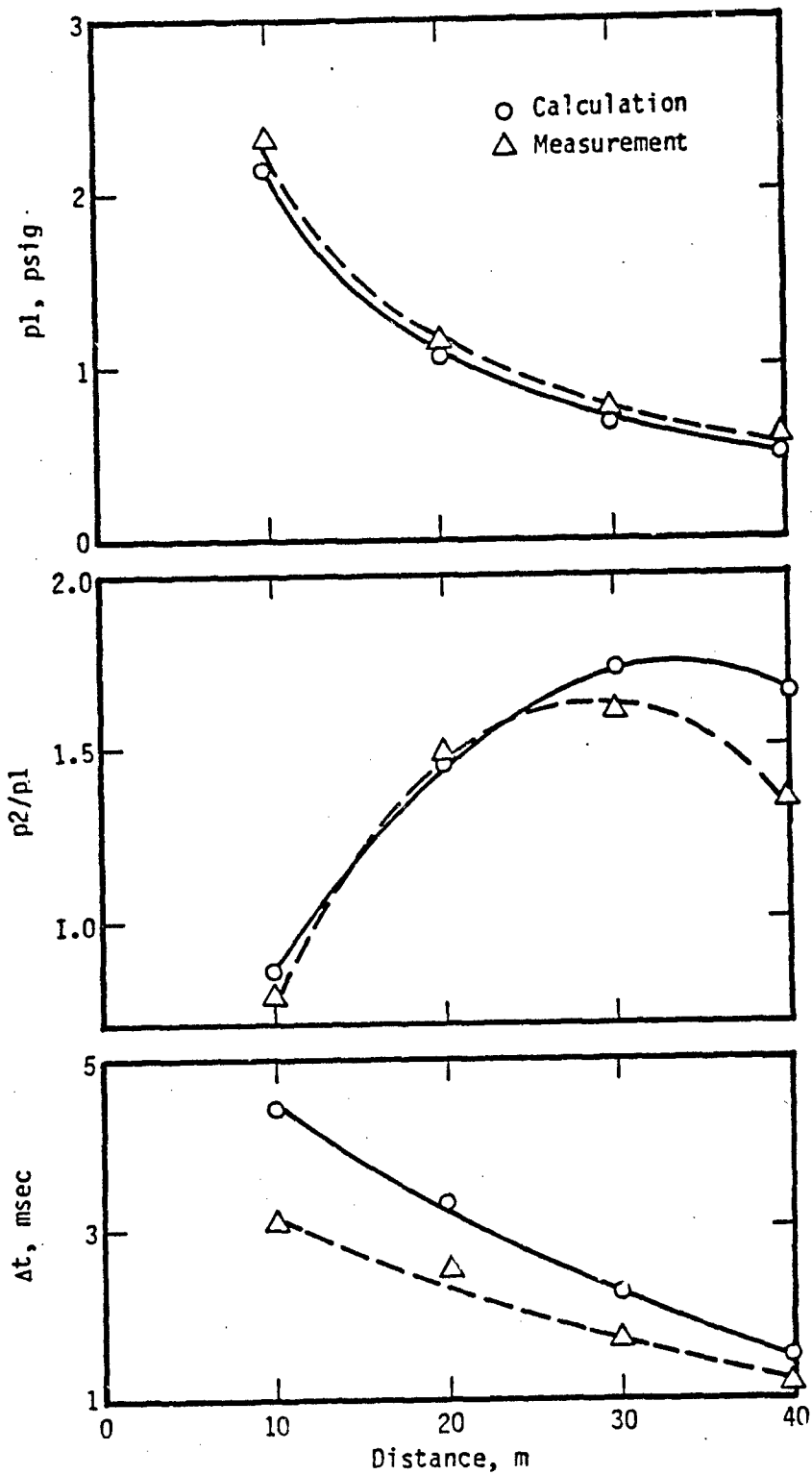
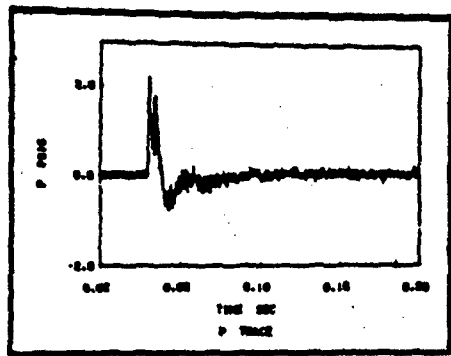
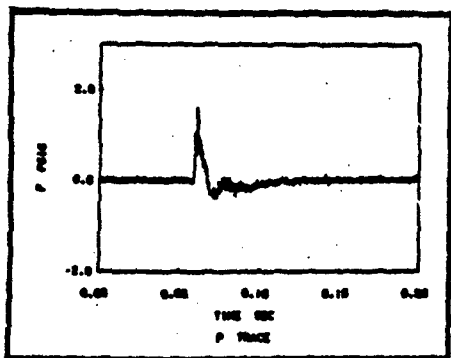
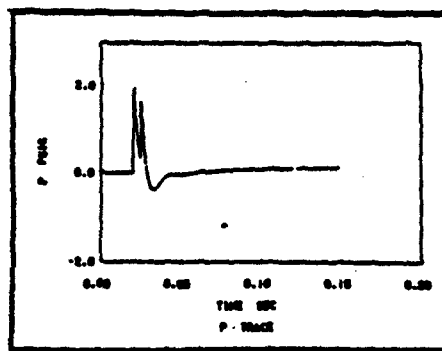


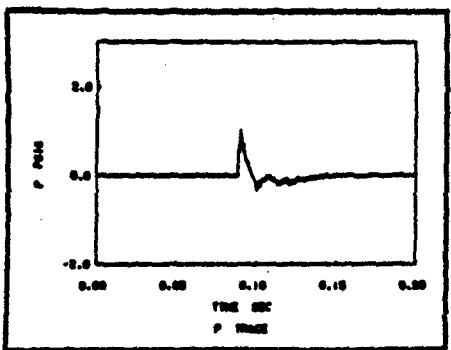
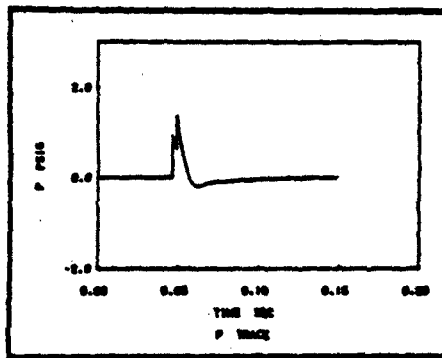
Figure 25. Variation of p_1 , p_2/p_1 and Δt with distance along 0° -line with 45° gun elevation



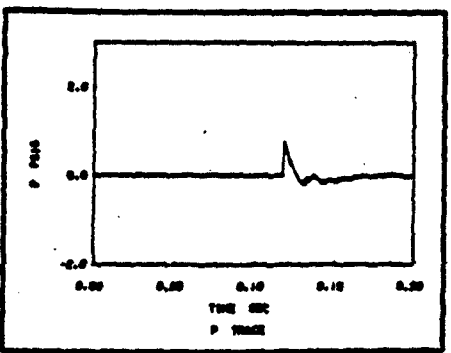
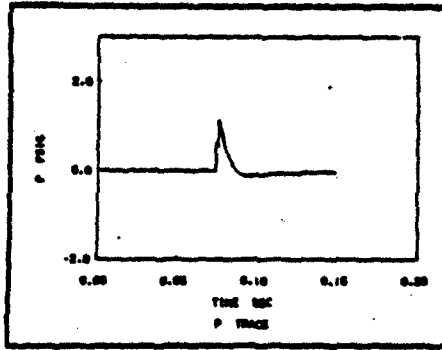
10m



20m



30m



40m

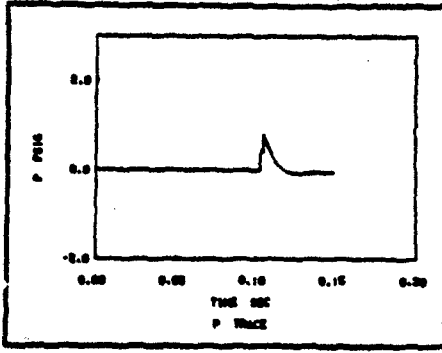


Figure 26. Measured and calculated pressure traces along 30°-line at 45° gun elevation

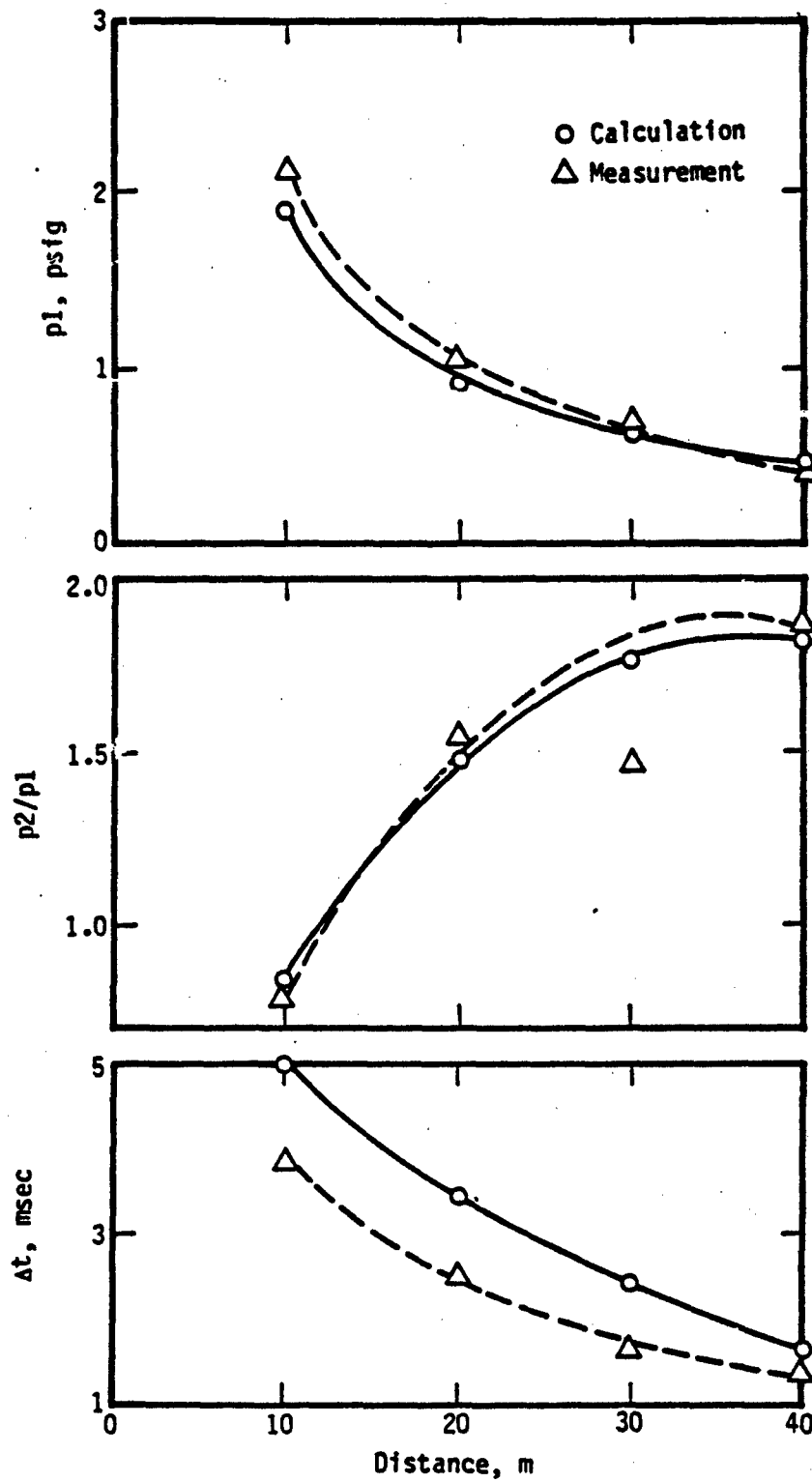
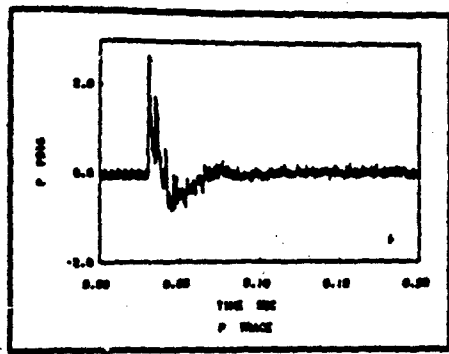
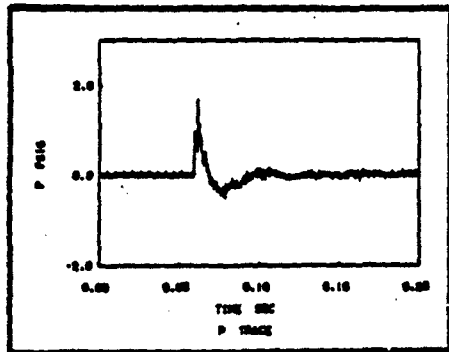
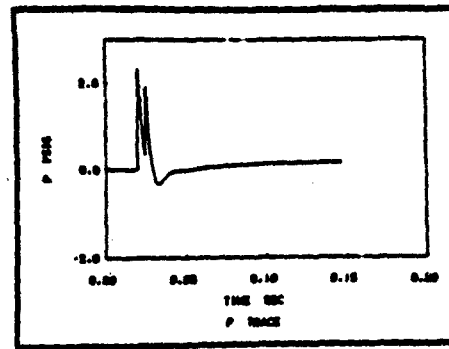


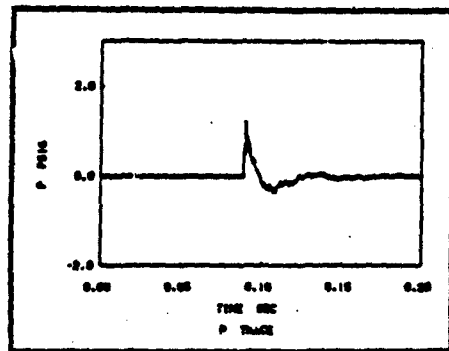
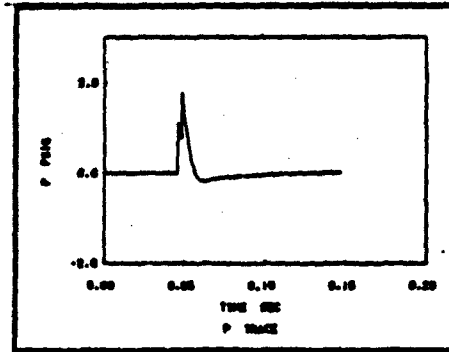
Figure 27. Variation of p_1 , p_2/p_1 and Δt with distance along 30°-line with 45° gun elevation



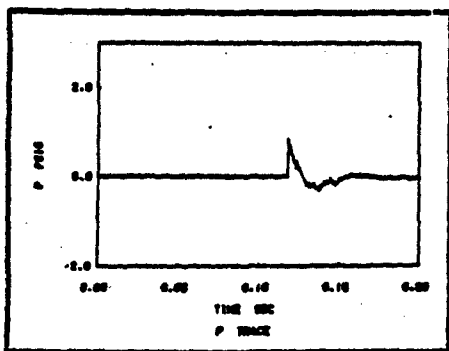
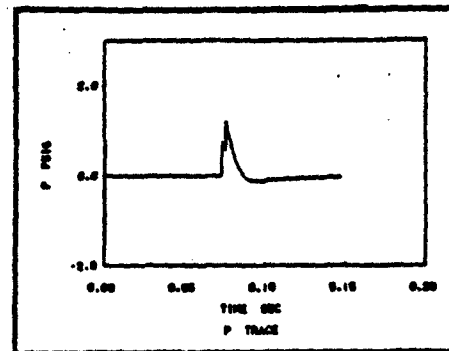
10m



20m



30m



40m

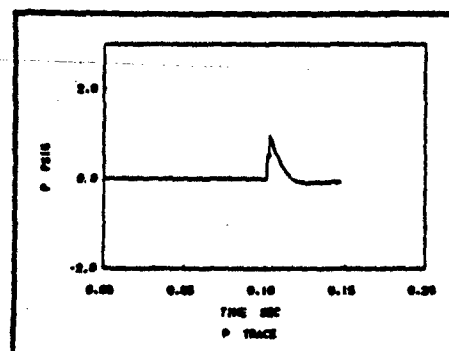


Figure 28. Measured and calculated pressure traces along 60°-line at 45° gun elevation

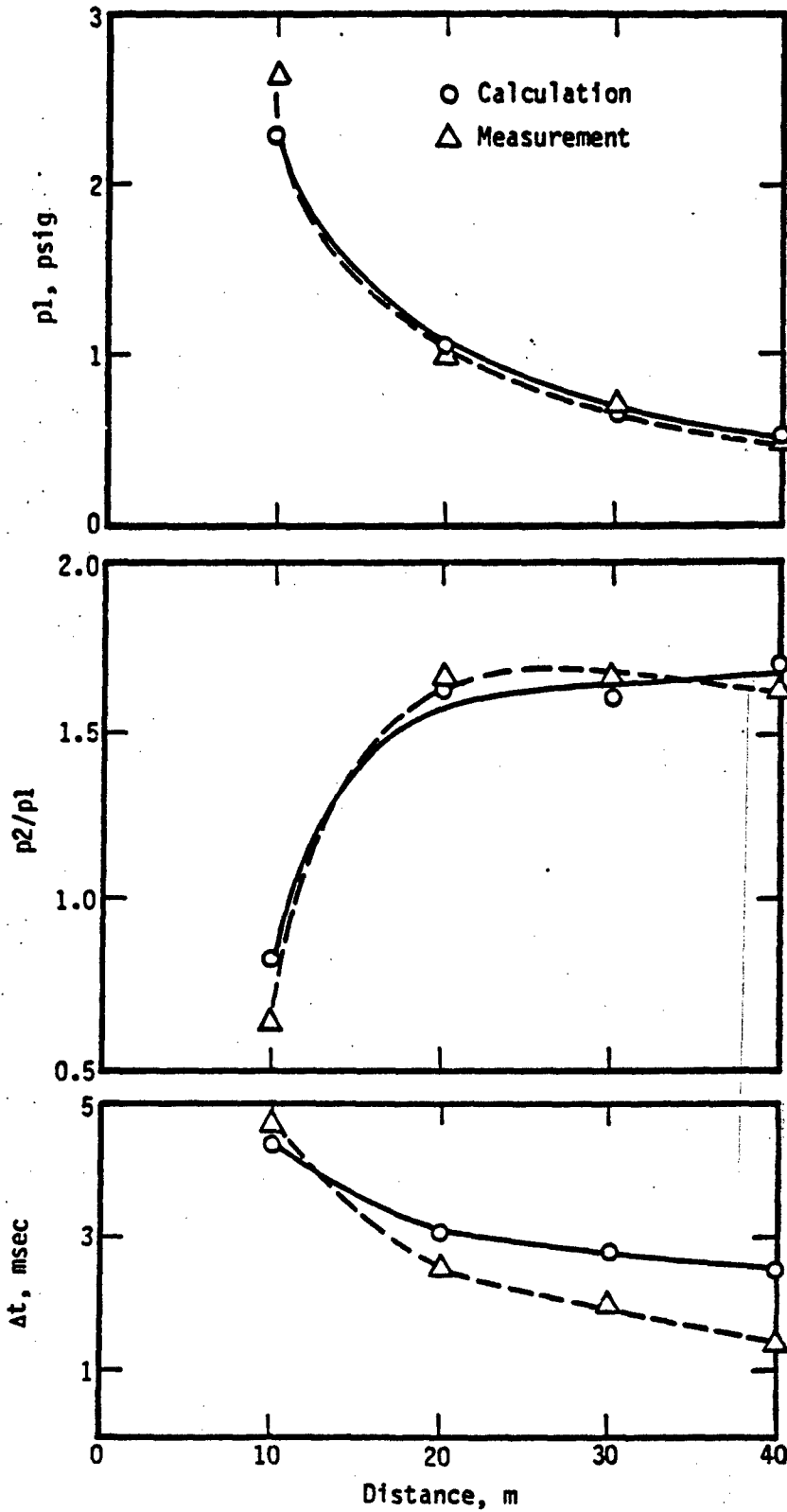
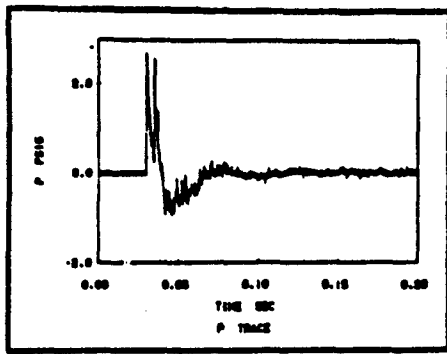
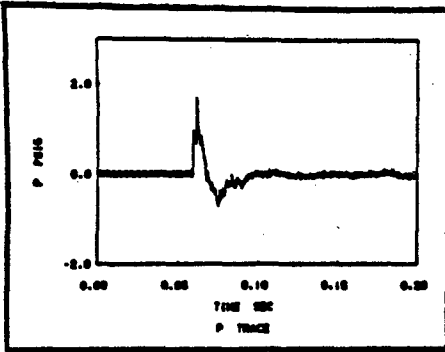
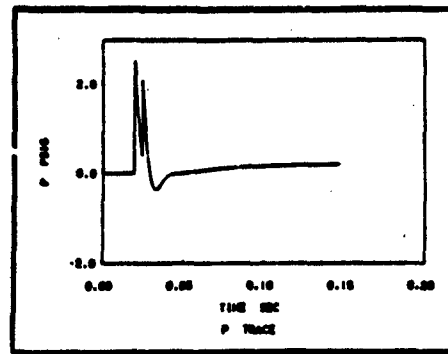


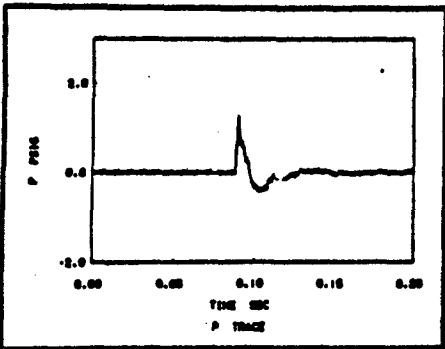
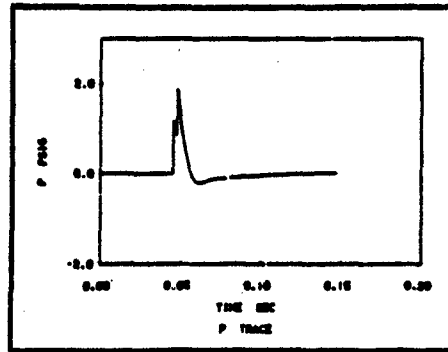
Figure 29. Variation of p_1 , p_2/p_1 and Δt with distance along 60° -line with 45° gun elevation



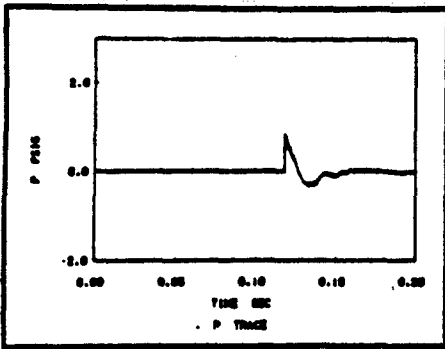
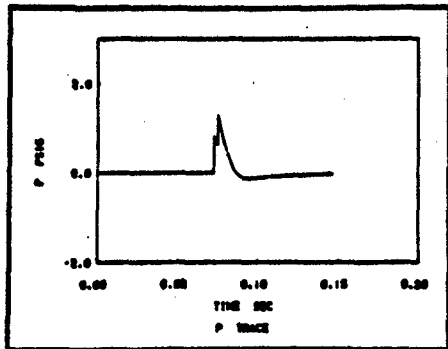
10m



20m



30m



40m

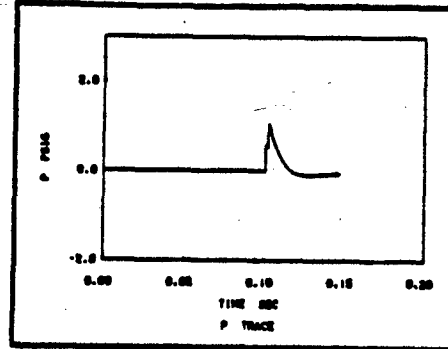


Figure 30. Measured and calculated pressure traces along 90°-line at 45° gun elevation

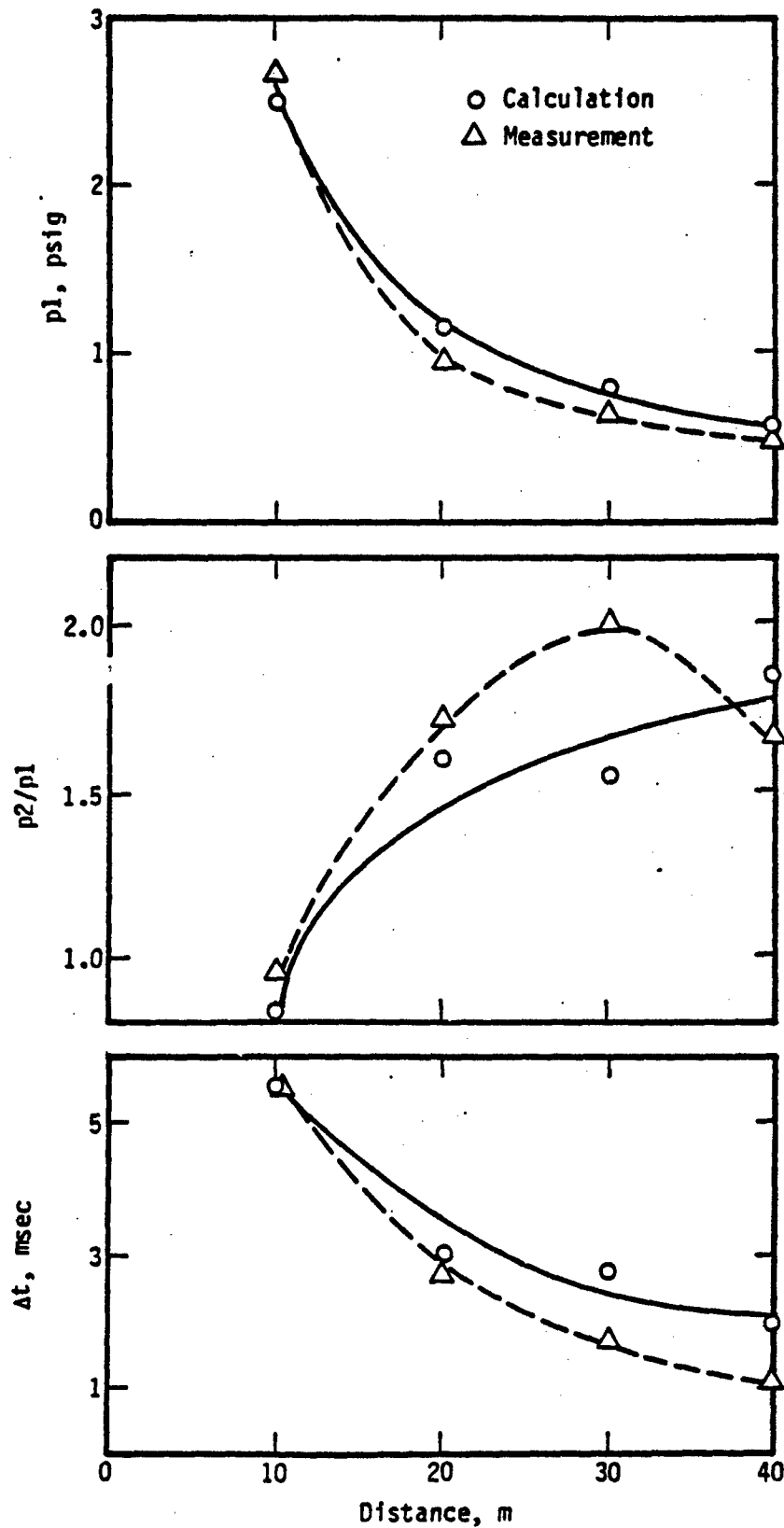
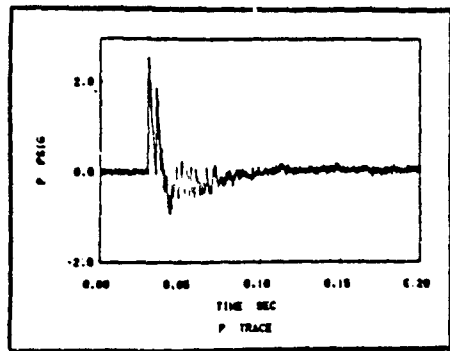
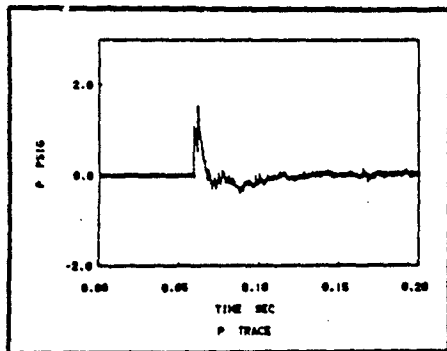
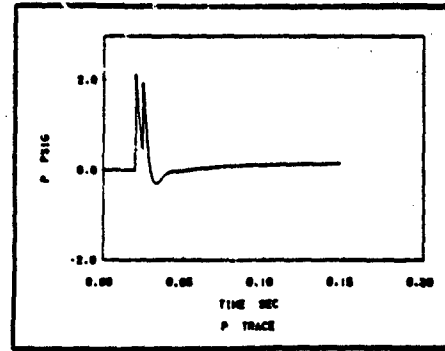


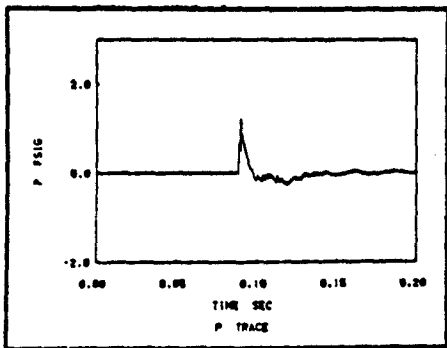
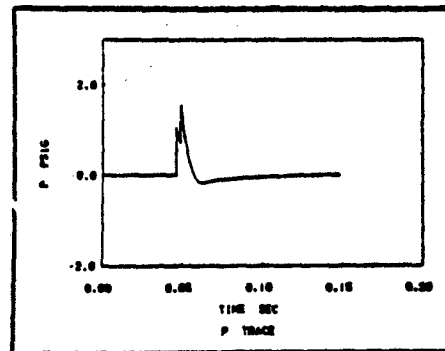
Figure 31. Variation of p_1 , p_2/p_1 and Δt with distance along 90°-line with 45° gun elevation



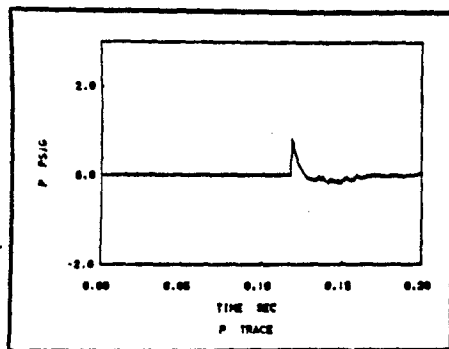
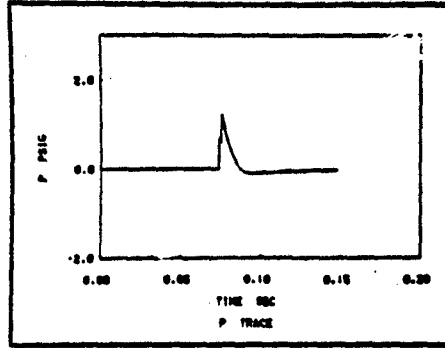
10m



20m



30m



40m

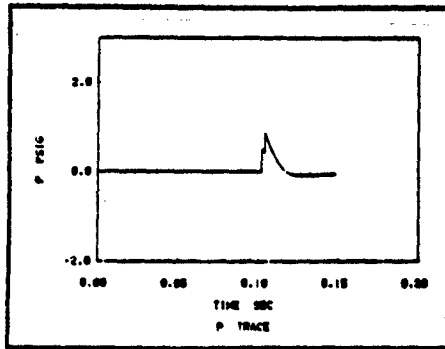


Figure 32. Measured and calculated pressure traces along 120°-line at 45° gun elevation

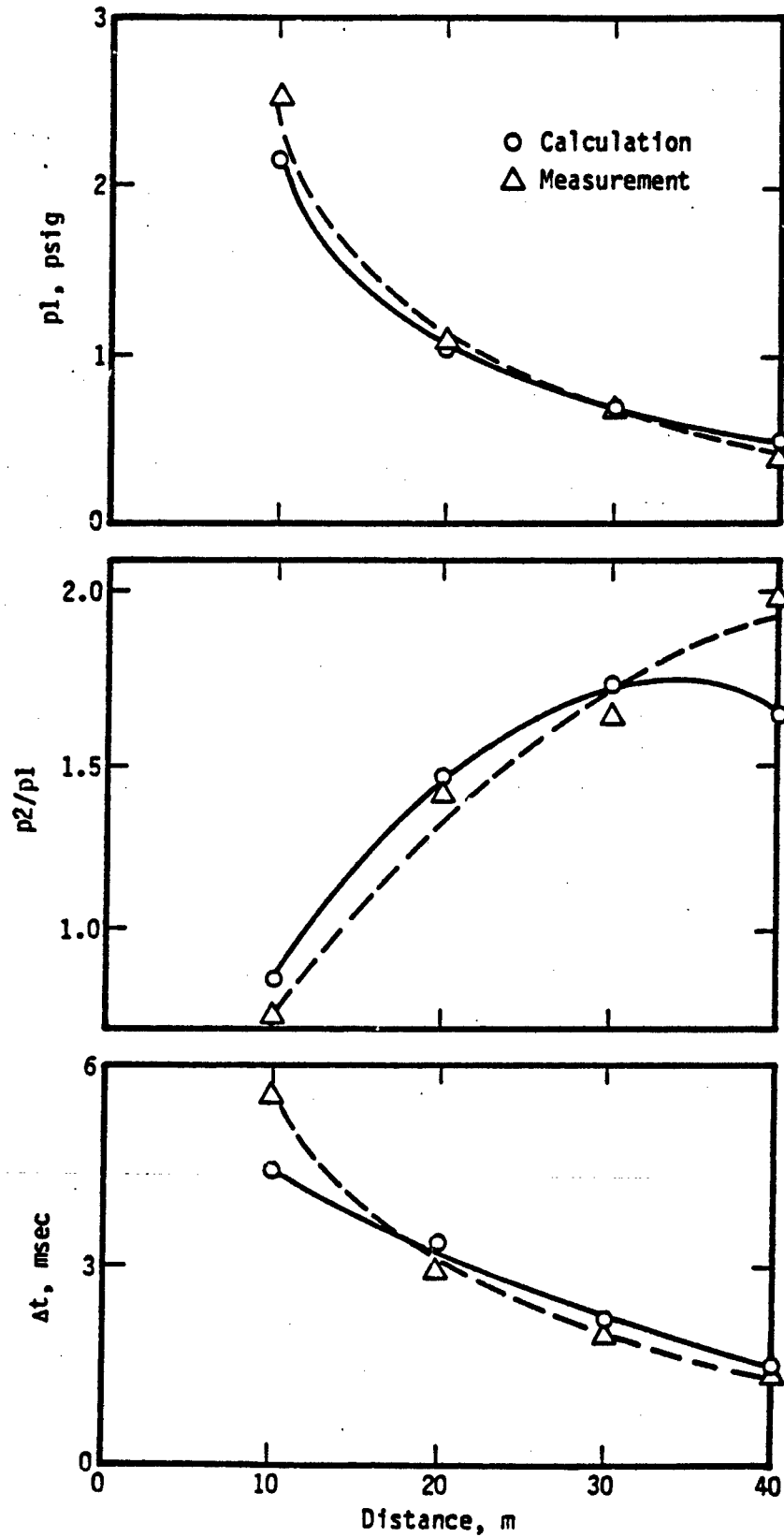
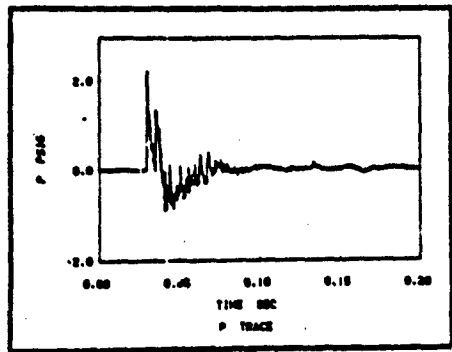
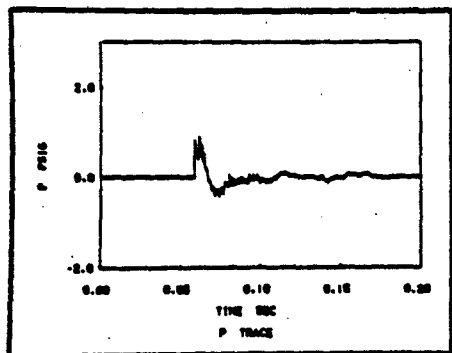
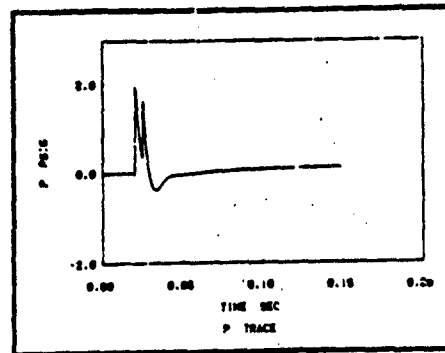


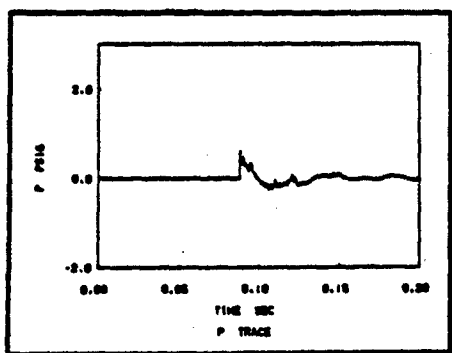
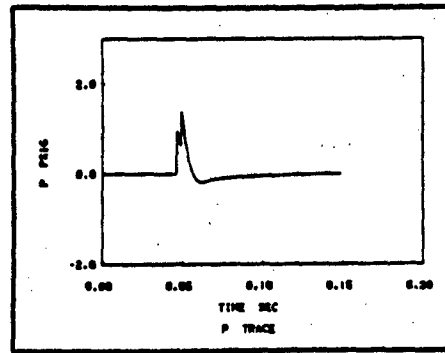
Figure 33. Variation of p_1 , p_2/p_1 and Δt with distance along 120° -line with 45° gun elevation



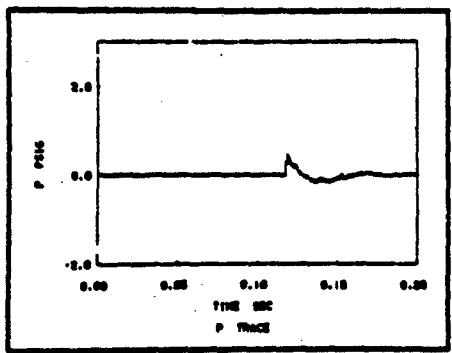
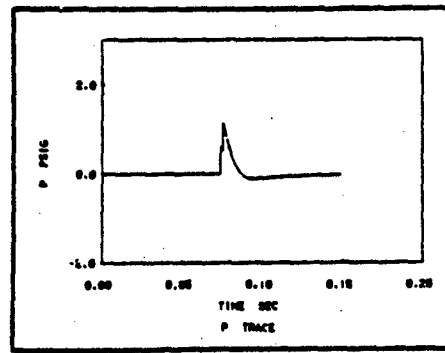
10m



20m



30m



40m

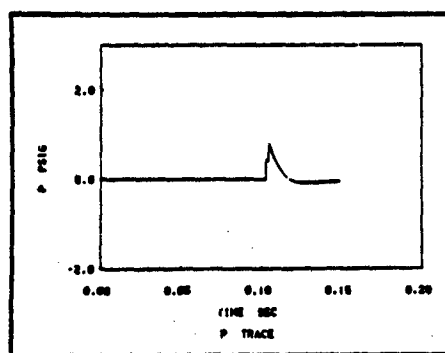


Figure 34. Measured and calculated pressure traces along 150°-line at 45° gun elevation

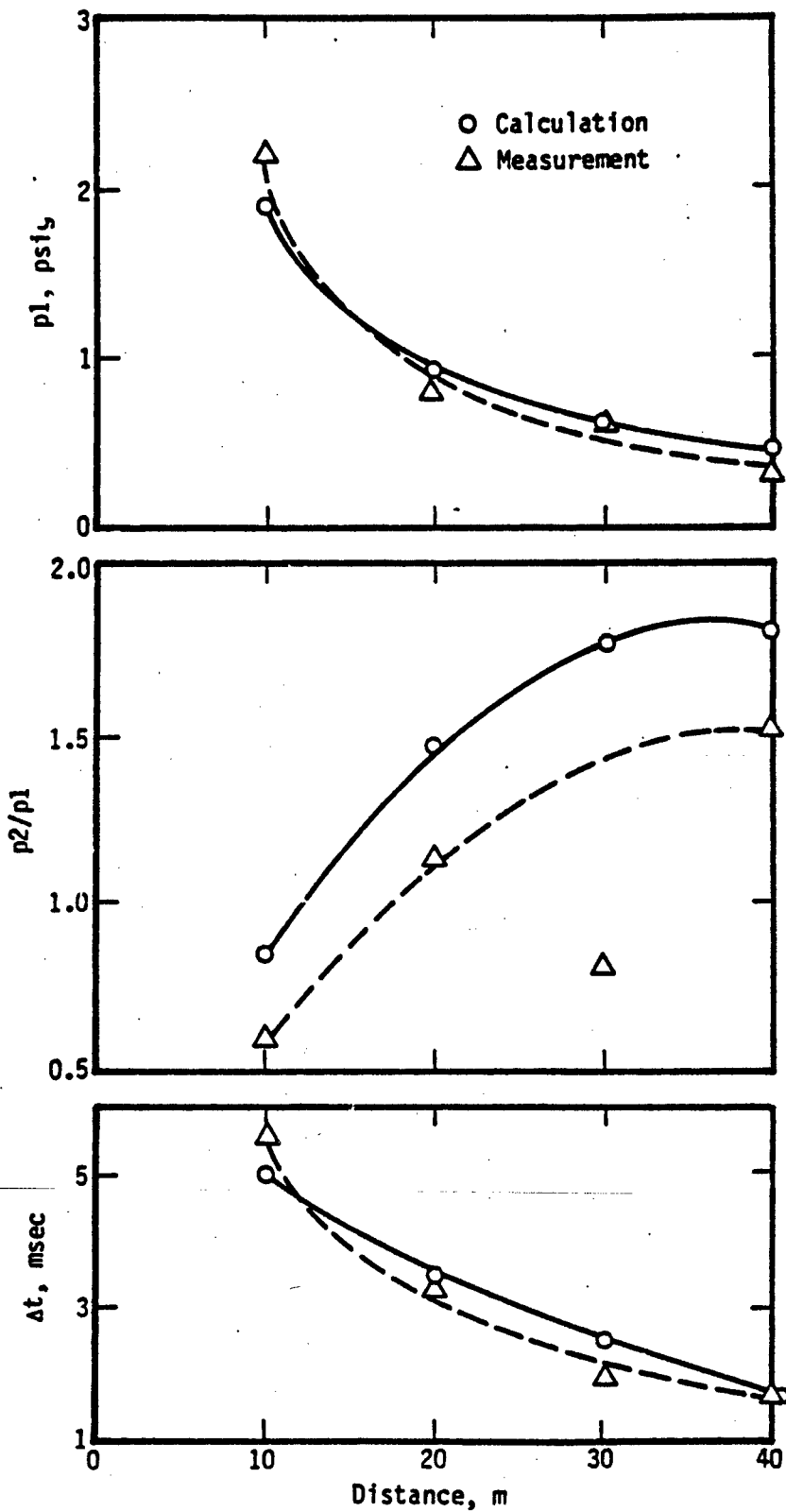


Figure 35. Variation of p_1 , p_2/p_1 and Δt with distance along 150° -line with 45° gun elevation

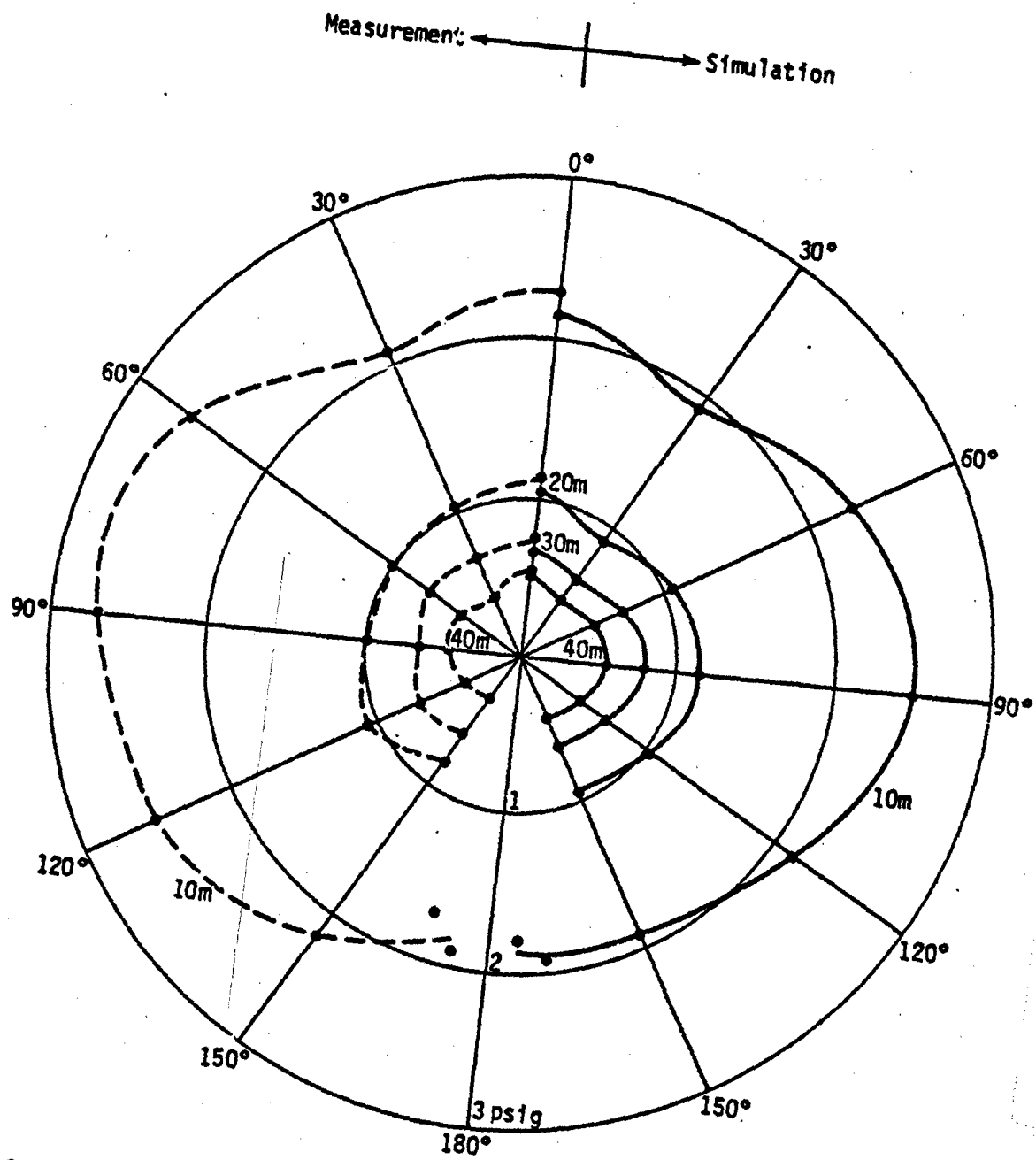


Figure 36. Comparison of calculated and measured p1 in the field at 45° gun elevation

APPENDIX A

A. GUN BLAST FAR FIELD ANALYSIS

A.1 INTRODUCTION

A gun blast wave is a physical phenomenon that occurs when the high pressure and high temperature product gas leaves the barrel after the explosion of the charge. The atmosphere is disturbed during and after the emergence of this gas. For the sake of clarity, we first consider the blast waves in a uniform unlimited medium, which can be treated as spherical since they result from release of a large amount of energy from a source of relatively small dimensions. The effects due to the wave reflection from the ground, the geometries of the gun and the muzzle brake, and so forth, will be considered in the following section.

At the front of the blast wave, the pressure p and density ρ jump abruptly from their undisturbed values. Immediately after the front passes, this disturbance decays to zero very fast and is followed by a rarefaction wave (Figure 37). The structure of the blast wave, e.g., the amplitude and the duration of both the compression and the rarefaction parts, varies according to its source strength and the ambient condition. Suppose the ambient condition is the standard atmosphere, then an extremely strong source, which results from, say, a nuclear explosion, will generate a strong blast wave. The

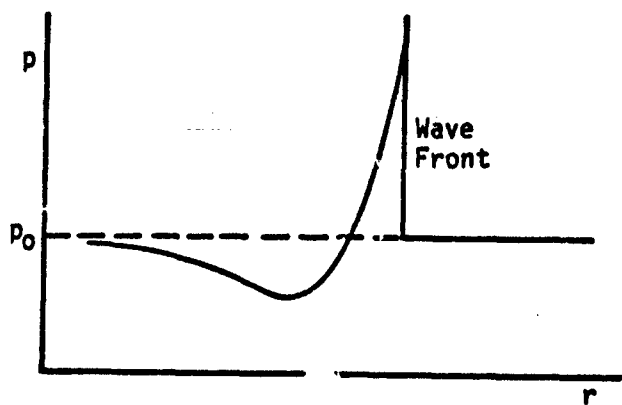


Figure 37. Spatial Pressure Distribution in Blast Wave

sound waves are essentially constant. Mathematically, it is much easier to treat the sound waves since the governing equations can be linearized by dropping higher order terms. Also, they reduce to a simple wave equation. The technique for solving this equation can be found in some of the standard textbooks (for example, Ref. 5).

Although human beings have used the gun powder for centuries, the blast wave theory has not been studied until World War II. Since then, a large amount of experimental as well as theoretical work has been done. Perhaps, the greatest progress was made when the concept of similarity was introduced independently by Sedov [1946, Ref. 6] and Taylor [1950, Ref. 7]. The concept has been used in other branches of fluid dynamics, such as boundary layer theory, conical flow theory, and transonic and hypersonic flow theory. The assumption of similarity decreases the number of independent variables and thus often reduces the governing partial differential equations to more manageable ordinary differential equations. It should be noted that similarity in the blast wave phenomenon does not hold exactly, but is valid only when the wave is strong enough to neglect the effect of the ambient atmospheric pressure. Nevertheless, the theoretical study of the blast wave phenomenon has to face the very difficult problem of finding the solution to the unsteady flow of the fully nonlinear gasdynamic equations, satisfying a moving boundary condition at the wave front. Analytical solution can be obtained only for very strong blast waves for which the similarity assumption can be justified.

For blast waves with intermediate source strength, numerical methods have to be employed for solving the gasdynamics equations. Probably one of the best methods is the method of characteristics which is applicable to hyperbolic type partial differential equations. We do not intend to go into the mathematical theory of hyperbolic equations, which may be found in several excellent works (for example, Ref. 8). However, we shall simply mention the main results needed for the computation. The distinguishing property of the hyperbolic equations is the existence of certain characteristic directions or lines in the r - t plane, usually called characteristics. It must be noted that the characteristic network is not known a priori, a result of the nonlinearity of the equations. Along the characteristics, the dependent variables satisfy a certain relation known as the compatibility relation. It provides the key to

the method of computation. Detailed procedures will be given in the following section.

In light of the experimental gun overpressure data collected for M198 Howitzer and M-203 charge, for example, see Figure 2, and the pressure traces shown in Figure 38, one can immediately identify that the gun blast waves are blast waves with intermediate source strength. It can be shown that, for the strong blast wave, the attenuation of the maximum pressure at the front behaves like r^{-3} while for the sound wave it behaves like r^{-1} [Ref. 5]. A systematic analysis of the experimental gun overpressure data indicates that the maximum overpressure attenuates like r^{-1} to r^{-2} .[†] Therefore, the validity of the assumption of the gun blast waves as blast waves with intermediate source strength is again indicated.

A.2 MATHEMATICAL FORMULATION

After the explosion of the charge, the shell is propelled by the high pressure and high temperature product gas, which leaves the muzzle brake as the shell is launched. Initially, the gas flow in a small region surrounding the muzzle brake is complicated by the geometries of the gun and the muzzle brake. This effect, however, becomes less significant further away. Suppose we choose the center of the muzzle brake as the origin, we can construct a spherical coordinates (r, θ, ψ) as shown in Figure 39.

[†]For instance, the following table shows the measured values of the amplitude of the incident wave obtained from the left column in Figure 32 and its comparison with the values obtained from the $\sim r^{-1}$ and $\sim r^{-2}$ relationships.

Distance Defined in Figure 1 (m)	Distance from the Muzzle Brake, r (m)	$\sim r^{-1}$ (psig)	Experimental (psig)	$\sim r^{-2}$ (psig)
10	11.44	1.41	2.50	4.98
20	20.76	0.78	1.06	1.51
30	30.51	0.53	0.71	0.71
40	40.38	0.40	0.40	0.40

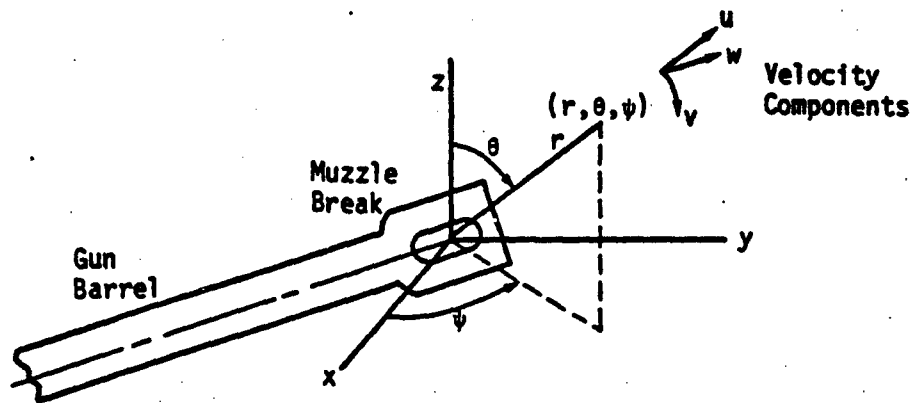


Figure 39. Spherical Coordinates with Origin at Center of Muzzle Brake

Assuming the gas is ideal, inviscid and it flows isentropically,* the equations of continuity, motion and energy can be written:

$$\frac{\partial \rho}{\partial t} + \frac{1}{r^2} \frac{\partial(\rho u r^2)}{\partial r} + \frac{1}{r \sin \theta} \frac{\partial}{\partial \theta} (\rho v \sin \theta) + \frac{1}{r \sin \theta} \frac{\partial}{\partial \psi} (w \rho) = 0 \quad (1)$$

$$\rho \left[\frac{Du}{Dt} - \frac{v^2 + w^2}{r} \right] = - \frac{\partial p}{\partial r} \quad (2)$$

$$\rho \left[\frac{Dv}{Dt} + \frac{uv}{r} - \frac{w^2 \cot \theta}{r} \right] = - \frac{1}{r} \frac{\partial p}{\partial \theta} \quad (3)$$

$$\rho \left[\frac{Dw}{Dt} + \frac{uw}{r} + \frac{vw \cot \theta}{r} \right] = - \frac{1}{r \sin \theta} \frac{\partial p}{\partial \psi} \quad (4)$$

$$\frac{D}{Dt} [p] = a^2 \frac{D}{Dt} [\rho] \quad (5)$$

where

$$\frac{D}{Dt} \equiv \frac{\partial}{\partial t} + u \frac{\partial}{\partial r} + \frac{v}{r} \frac{\partial}{\partial \theta} + \frac{w}{r \sin \theta} \frac{\partial}{\partial \psi}$$

*Isentropic assumption is not valid for the shock wave associated with the strong blast for which the Rankine-Hugoniot shock relations have to be employed to account for the entropy jump, but it is valid here.

Here u , v and w are the velocity components, p is the pressure, ρ is the density, a is the local sonic speed, and t is the time measured from the instant that the blast waves are generated.

A complete solution to Equations (1) to (5) depends on the source distribution in the muzzle brake which in turn depends on the detonation of the explosive charge and its resulting flow field in the barrel. However, for the present study, our primary goal is to establish the feasibility of obtaining the solution of the pressure traces at different far field positions by solving the gasdynamics equations. Instead of attempting to solve the complex barrel flow, we simulate the origin of the blast waves as a sphere of pressurized gas. Furthermore, we assume that the transport processes are important only along the radial direction and those associated with θ and ψ directions are secondary. This assumption is justified by the sound comparison of our results with the experimental data, as given in Section 2. With these assumptions, Equations (1) to (5) can be simplified as follows:

$$\rho_t + u\rho_r + \rho\left(u_r + \frac{2u}{r}\right) = 0 \quad , \quad (6)$$

$$u_t + uu_r + \frac{1}{\rho} p_r = 0 \quad , \quad (7)$$

$$p_t + up_r - a^2(\rho_t + u\rho_r) = 0 \quad , \quad (8)$$

where the subscript t and r denote partial differentiation. Here Equations (3) and (4) are neglected since these equations describe secondary phenomena.

The initial and boundary conditions to Equations (6) and (8) can be written as

At $t = 0^-$,

$$\left. \begin{array}{l} p = p_s \\ \rho = \rho_s \\ a = a_s \\ u = 0 \end{array} \right\} \text{for } r < r_0 \quad (9)$$

$$\left. \begin{array}{l} p = p_o \\ \rho = \rho_o \\ a = a_o \\ u = 0 \end{array} \right\} \text{for } r > r_0 \quad (10)$$

where r_0 = initial radius of the pressurized gas sphere, and the subscripts s and o denote source and undisturbed conditions, respectively.

At $t > 0^+$,

$$u = 0 \quad \text{at } r = 0 \quad (11)$$

Since Equations (6) to (8) are hyperbolic equations [Ref. 8], their characteristic form can be obtained in the following way. First, let us define

$$\sigma \equiv \int \frac{dp}{\rho a} \quad (12)$$

Substitution of Equation (12) into Equations (6) to (7) yields

$$\sigma_t + u\sigma_r + a u_r + \frac{2au}{r} = 0 \quad (13)$$

$$u_t + uu_r + a\sigma_r = 0 \quad (14)$$

Adding and subtracting Equation (13) with Equation (14), we obtain

$$(\sigma + u)_t + (u + a) (\sigma + u)_r + \frac{2au}{r} = 0 \quad (15)$$

$$(\sigma - u)_t + (u - a) (\sigma - u)_r + \frac{2au}{r} = 0 \quad (16)$$

respectively. It may be shown that for isentropic flow

$$\sigma = \frac{2a}{\gamma - 1} \quad (17)$$

Equations (15), (16) and (8), with the substitution of Eq. (17), can then be cast into characteristic form as follows

On r^+ curve:

$$\left\{ \begin{array}{l} \frac{dr}{dt} = u + a \end{array} \right. \quad (18)$$

$$\left\{ \begin{array}{l} \frac{d}{dr} \frac{2a}{\gamma - 1} + u + \frac{2au}{r} = 0 \end{array} \right. \quad (19)$$

On r^- curve:

$$\left\{ \begin{array}{l} \frac{dr}{dt} = u - a \end{array} \right. \quad (20)$$

$$\left\{ \begin{array}{l} \frac{d}{dr} \frac{2a}{\gamma - 1} - u + \frac{2au}{r} = 0 \end{array} \right. \quad (21)$$

On r^0 curve:

$$\left\{ \begin{array}{l} \frac{dr}{dt} = u \end{array} \right. \quad (22)$$

$$\left\{ \begin{array}{l} \frac{dp}{dr} - a^2 \frac{d\rho}{dr} = 0 \end{array} \right. \quad (23)$$

Equations (18), (20) and (22) define the direction of the characteristics r^+ , r^- and r^0 respectively. Along these characteristics, the compatibility relations, e.g., Equations (19), (21) and (23), are satisfied accordingly. A sketch of r^+ , r^- and r^0 characteristics are shown in Figure 40. It should be noted that the characteristics r^0 are identical to the streak lines of the fluid particle. Furthermore, the blast wave front follows closely with one of the r^+ characteristics.

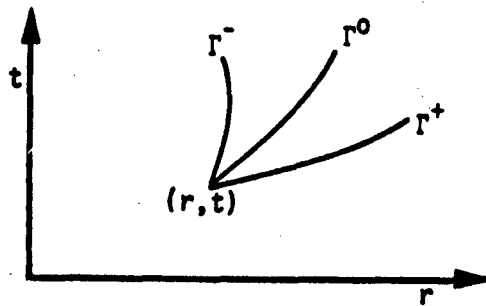
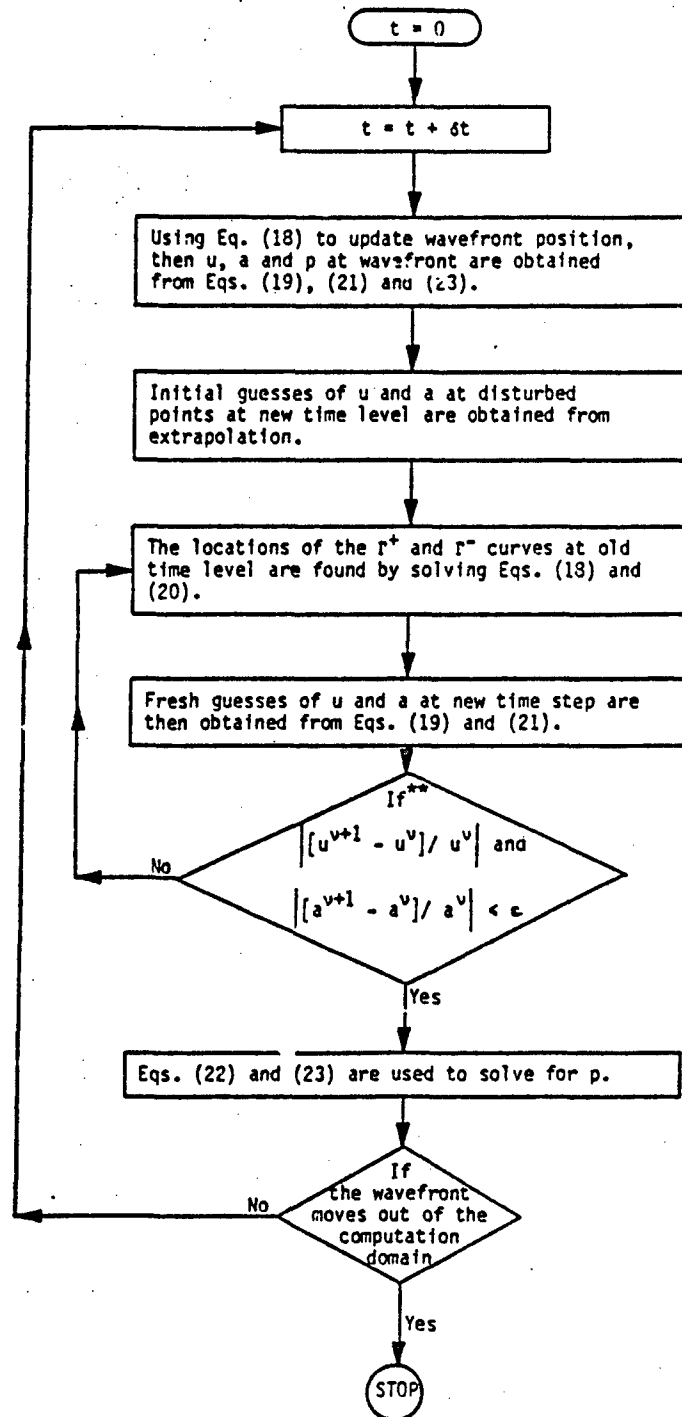


Figure 40. Characteristics in r-t Plane.

Since Equations (18) to (21) consist of only two unknown variables u and a , these equations are solved first. Once u and a are found, Equations (22) and (23) can be used to obtain the solution of p after the substitution of $\rho = \gamma p/a^2$. The solution of the characteristic equations, Eqs. (18) to (21), is based on the upstream interpolation scheme introduced by Belotserkovskii and Chushkin [Ref. 9]. The basic idea is as follows: Firstly, approximate those equations by use of first order implicit finite difference formula for small time steps, which results in a piecewise linear characteristic network. The wave front is traced by following one of the r^+ characteristics, initiated at the boundary of the pressurized gas sphere. This particular characteristic divides the disturbed flow region from the undisturbed one. A number of points in r -direction with equal spacing δr are used. The exact number depends on how far from the muzzle brake we want to calculate. Old convergent solutions are extrapolated to give initial guesses for flow variables at new time level. They are substituted into Equations (18) and (20) which give roughly the locations of the r^+ and r^- curves at old time level. Hence flow variables at these locations can be determined by interpolation between the convergent solutions at the old time level. With this information fresh values at new time locations are obtained from Equations (19) and (21). Due to the implicit nature of the method, the process is iterated until two successive guesses of the flow variables at the new time step agree within sufficiently close limits. The solution procedure can be summarized in the following flow chart (Figure 41).



**The superscript v denotes the v th iteration, and ϵ is the tolerance limit of relative error for convergence.

Figure 41. Flow Chart for the Method of Characteristics.

The wave reflection from the ground will generate another peak in the pressure traces (see Figure 2) due to different times of arrival of the incident wave and the reflected wave. The way to calculate the reflected wave is similar to those used in the geometrical optics. The paths of the incident and reflected waves are shown schematically in Figure 42. Here O , H , PS and θ denote the center of the muzzle brake, its height, location of the pressure sensor, and the angle of incident and reflection with respect to the normal from the ground. It must be noted that the two angles are identical which guarantees only a single reflected wave can go through the point PS . Following the procedure commonly used in the geometrical optics, the reflected wave can be regarded as another spherical wave generated by a mirror image of the muzzle brake. Then the solution from the method of characteristics is used simultaneously for both the incident and reflected waves according to their path lengths. Since the pressure is a scalar quantity, its value at a certain point and at a certain instant is obtained by summing the contributions from the two waves. Strictly speaking, a superposition procedure is not valid for nonlinear equations, Equations (6) to (8). However, the difference of the times of arrival for the two signals is small compared with the time scale of the blast wave. The nonlinear effect is thus neglected here in obtaining a first order solution. Refinements will be considered later.

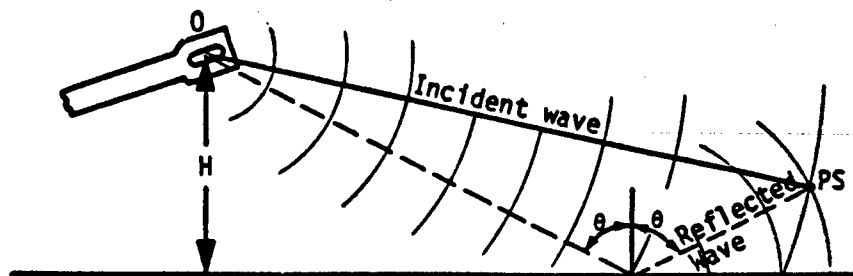


Figure 42. Paths of Incident and Reflected Waves.

B. MATHEMATICAL MODEL OF LUNG

B.1 INTRODUCTION

Gun blast injury is a complex phenomenon and might be very hazardous to the crews who operate the gun. The important clinical, pathological and physiological information, regarding the effects of direct air-blast injury on the biologic subject, has been extensively reviewed (for instance, References 10 and 11). In order to quantify the damage to the lung due to blast overpressure, a mathematical model (Refs. 1 and 12) was proposed to study the body-dynamical and gas-dynamical responses of the thoraco-abdominal structures. In the present study, we utilize this model as a mathematical tool to analyze the lung response on the crew positions, resulting from the measured and our calculated blast overpressures respectively.

B.2 MATHEMATICAL FORMULATION

The lung is simulated as a gas-filled cavity whose volume represents the total of the alveolar and bronchial gas (Figure 43). The gas in the lung is assumed to behave as an ideal gas and is homogeneous in pressure. Furthermore, the thoracic and abdominal walls are assumed to be perfectly rigid. The effect on lung volume of chest-wall and diaphragmatic action is simulated by means of two piston systems. Essentially, the inertia, stiffness, tissue resistance, and surface area of the chest wall and abdomen are the determinate factors of this action. In fact, these various factors are included in the simulation of each piston as a simple system consisting of a mass, spring, damping friction and effective area. Apart from the above-mentioned assumptions, linear response of the spring is assumed to render our calculation within the elastic limit. The equations governing the motion of the pistons are written as follows

$$M_c \ddot{x}_c + C_c \dot{x}_c + \kappa_c x_c = A_c (p - p_g) \quad (24)$$

$$M_a \ddot{x}_a + C_a \dot{x}_a + \kappa_a x_a = A_a (p - p_g) \quad (25)$$

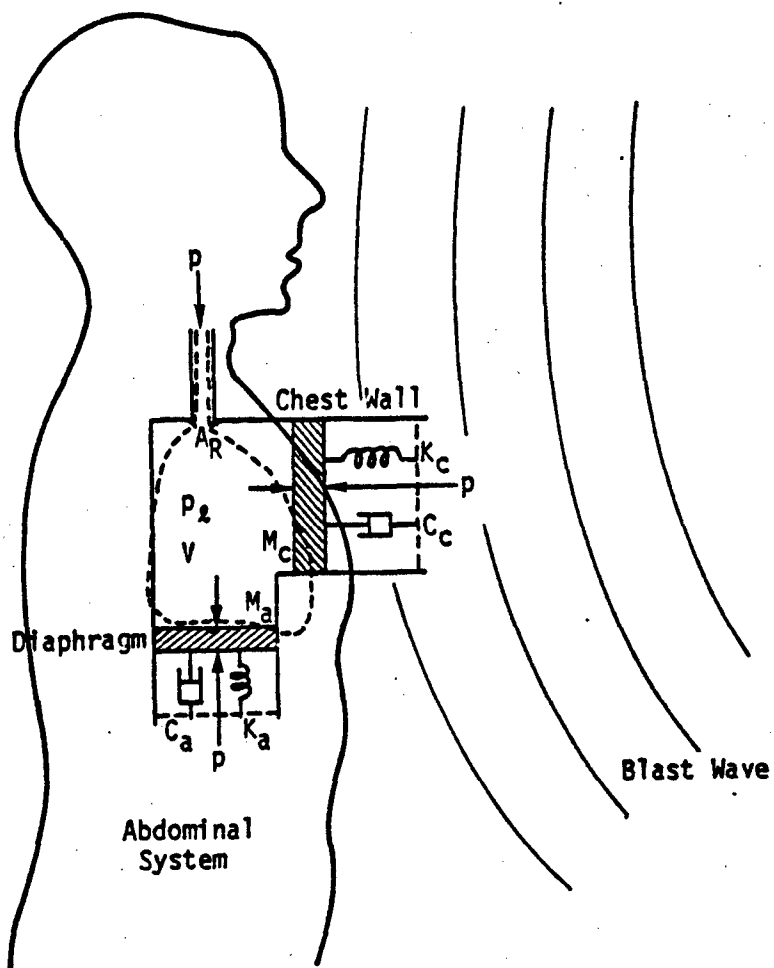


Figure 43. Definition sketch of lung model

Here M , C , κ , χ , A and p are the mass, damping coefficient, spring coefficient, linear displacement, effective area and the pressure. The subscripts c , a and l denote the chest-wall, abdomen and lung, respectively.

The gas flow through the respiratory passageways and openings is approximated by an orifice whose geometric area is the effective area presented by the respiratory openings to the air flow (Figure 43). The gas in the lung is compressed or expands adiabatically in accordance with the motion of the pistons and it escapes from or enters into the lung cavity through the orifice. The rate of change of lung pressure can be described in the following equation,

$$\frac{dp_l}{dt} = -\frac{\gamma p_l}{V} \frac{dV}{dt} + \text{Sgn}(p - p_l) \frac{A_r \sqrt{|p - p_l|}}{V \cdot \alpha}, \quad (26)$$

where

$$V = V_0 - \chi_a A_a - \chi_c A_c,$$

$$\text{Sgn}(p - p_l) = \begin{cases} +1, & \text{if } p > p_l \\ -1, & \text{if } p < p_l \end{cases},$$

$$\alpha = 6 \times 10^{-4} \text{ an empirical constant.}$$

Here V denotes the gaseous volume of the lung, A_r denotes the effective area of the orifice, γ denotes the ratio of the specific heats, and V_0 denotes the undisturbed lung volume. The first term in the right hand side of Equation (26) represents the adiabatic compression process while the second term is obtained empirically for compressible flow through an orifice. It should be noted that the driving force of Equations (24) to (26) is the difference between the external blast pressure and the lung pressure acting upon the cross-sectional area of the orifice and the piston areas.

The various coefficients used in Equations (24) to (26) are obtained from dimensional analysis based on the measured values from a 2.2 kg rabbit (Ref. 12). The inherent assumption in the dimensional analysis is the similarity of tissue density, tissue elasticity and body shapes among all animal species. The evaluated results for a 180 lb. man are summarized in the table below.

<u>Coefficients</u>	<u>Units</u>	<u>Value for 180 lb Man</u>
M_c	lb	0.8906
M_a	lb	3.7850
A_c	ft ²	0.2893
A_a	ft ²	0.1113
C_c	Poundal-sec/ft	2.7820×10^2
C_a	Poundal-sec/ft	1.1130×10^2
κ_c	Poundal/ft	1.2170×10^3
κ_a	Poundal/ft	3.7860×10^3
V_o	ft ³	2.9180×10^{-2}
A_r	ft ²	1.9030×10^{-4}

Subsequently, Equations (24) to (26) are solved numerically by a fourth order Runge-Kutta method.

REFERENCES

1. Holladay, A. E. and Bowen, I. G., "A Mathematical Model of the Lung for Studies of Mechanical Stress," Proc. of the San Diego Symp. for Biomedical Engr. 1963, 39-50.
2. Newton, I., Philosophiae Naturalis Principia Mathematica (London, 1726), Book II, Proposition 50.
3. Laplace, P. S. de, "Sur la vitesse du son dans l'air et dans l'eau," Annales de Chimie et de Physique, Series 2, 3 (1816), 238-241.
4. Liepmann, H. W. and Roshko, A., "Elements of Gasdynamics," (1956), Wiley, New York.
5. Whitham, G. B., "Linear and Nonlinear Waves," 1974, John Wiley & Sons, New York.
6. Sedov, L. I., (1946). Compt. Rend. Acad. Sci., URSS 52, 1, 17.
7. Taylor, G. I. (1950). Proc. Roy. Soc. (London), A201, 159.
8. Courant, R. and Friedrichs, K. O., "Supersonic Flow and Shock Waves," (1948), Wiley (Interscience), New York.
9. Belotserkovskii, O. M. and Chushkin, P. I., "The Numerical Solution of Problems in Gas Dynamics," (1965), in Basic Developments in Fluid Dynamics, (ed., M. Holt), Vol. 1, Academic Press, New York.
10. Clemenson, C.-J., "Blast Injury," (1956), Physiol. Rev. 36: 336-354.
11. Chiffelle, T. L., "Pathology of Direct Air-Blast Injury," (1966), DASA-1778, Lovelace Foundation for Medical Education and Research, Albuquerque, New Mexico.
12. Bowen, I. G. and Holladay, A. E., "A Fluid-Mechanical Model of the Lung for Studies in Blast Biology," Proc. of the San Diego Symp. for Biomedical Engr. 1962, 142-149.

CONTRACT PUBLICATION AND PERSONNEL

Publications and personnel supported by this contract. Test Planning collection, and Analysis of Pressure Data Resulting from Army Weapon Systems - are listed in chronological order by volume, subject matter and personnel contributing to the effort.

November 1979 - Volume I -	Pure Tone Audiograms for Minipigs - Dr. William M. Jenkins Mr. Henry C. Evans, Jr.
April 1980 - Volume II -	Modeling of Far Field Data Dr. J. Stuhmiller Dr. F. Chan Dr. P Masiello M(s) K. Tani
May 1980 - Volume III -	A Correlation Window for the M198 Howitzer Dr. Steve Slinker Mr. Henry C. Evans, Jr.
May 1980 - Volume IV -	Data Analysis of the M198 and M109 May 1979 Firings Dr. Steve Slinker Dr. Henry C. Evans, Jr.
May 1980 - Volume V -	Shock Tube Analysis and Correlation Study Dr. Steve Slinker Mr. Henry C. Evans, Jr. M(s) Carol Jordon

DISTRIBUTION LIST

12 Copies

Director (ATTN: SGRD-UWZ-C)
Walter Reed Army Institute of Research
Walter Reed Army Medical Center
Washington, DC 20012

4 Copies

USAMRDC (SGRD-RMS)
Fort Detrick
Frederick, MD 21701

12 Copies

Defense Technical Information Center (DTIC)
ATTN: DTIC-DDA
Cameron Station
Alexandria, VA 22314

1 Copy

Dean
School of Medicine
Uniformed Services University
of the Health Sciences
4301 Jones Bridge Road
Bethesda, MD 20014

1 Copy

Commandant
Academy of Health Sciences, US Army
ATTN: AHS-CDM
Fort Sam Houston, TX 78234